Abid Saleem

Design and optimization of a magnet pole for Magnetic Resonant Imaging

School of Electrical Engineering

Thesis submitted for examination for the degree of Master of Science in Technology.

Espoo 20.04.2018

Thesis supervisor:

Prof. Anouar Belahcen

Thesis advisor:

Victor Mukherjee, M.Sc

Aalto University
School of Electrical
Engineering

AALTO UNIVERSITY
SCHOOL OF ELECTRICAL ENGINEERING

ABSTRACT OF THE
MASTER'S THESIS

Author: Abid Saleem

Title: Design and optimization of a magnet pole for Magnetic Resonant Imaging

Date: 20.04.2018 Language: English Number of pages:6+48

Department of Electrical Engineering and Automation

Professorship: Electromechanics Code: S-17

Supervisor: Prof. Anouar Belahcen

Advisor: Victor Mukherjee, M.Sc

Magnetic resonance imaging (MRI) devices require a uniform magnetic field in the measuring area to capture the high-quality images. Permanent magnets are widely used as the main field source in the MRI devices. The field produced by such magnets is not uniform. Therefore, different field correction methods are usually employed to increase the uniformity of the magnetic field. In this thesis, a two dimensional (2-D) and three dimensional (3-D) numerical model of an MRI device is developed. The design and optimization of the poles for a low field MRI device is performed by using 2-D finite element (FE) method to increase the magnetic field uniformity. The pole faces are modelled by using non-uniform rational b-splines (NURBs). The particle swarm optimization algorithm is used to optimize the pole faces and magnet design of the MRI device. The optimization of different parameters of the pole surface is performed and compared for the homogeneity of the magnetic field in the measuring area. Finally, the best choice is made based on the field uniformity and minimum weight of the assembly. The final optimized design achieved from the 2D FE model is further compared with the 3D FE model. Moreover, the selected design is subjected to the sensitivity analysis to account for the magnetic field tolerances. Furthermore, the structural analysis is performed to take into account the effect of the stress ensuring that the designed structure is stiff enough to sustain the heavy mass without causing any deformation.

Keywords: Magnetic Resonant Imaging, Non Uniform rational b spline , Particle swarm optimization, Finite element method.

Preface

It is my privilege and honour to express my most profound gratitude to my supervisor Prof. Anouar Belahcen for his constructive supervision during the accomplishment of this research project. It has been an utmost pleasure working under his supervision. I would like to thank my advisor Victor Mukherjee for his valuable suggestions and helping throughout my thesis.

Finally, I would like to thank my parents, Mr. Sheikh Saleem Akhter and Mrs. Ansar Saleem, my brothers Dr. Hamid and Dr. Saad for their consistent support, love and sincere prayers.

Espoo, 20.04.2018

Abid Saleem

Contents

Symbols and Abbreviations

Symbols

$\mathbf{A}$	Magnetic vector potential
$\mathbf{B}$	Magnetic flux density
B_o	Main magnetic field
B_1	Radio frequency field
B_2	Gradient field
B_{avg}	Average magnetic field
B_{min}	Minimum value of magnetic field
B_{max}	Maximum value of magnetic field
B_r	Remanence flux density
H	Magnetic field intensity
H_{ci}	Intrinsic coercive force
H_c	Coercive force
T_c	Curie temperature
V_m	Magnetic scalar potential
μ_o	Permeability in vacuum
μ_r	Relative permeability

Abbreviations

$2D$	Two dimensional
$3D$	Three dimensional
DSV	Diameter of spherical volume
FEM	Finite element method
GA	Genetic algorithm
MRI	Magnetic resonance imaging
$NdFeB$	Neodymium Iron Boron
$NURBS$	Non-uniform rational B spline
PSO	Particle swarm optimization

Chapter 1

1 Introduction

Healthcare industries are always looking for innovative ideas and designs to implement the technology that can contribute to the wellness of people. Diagnosing the disease, storing the patient's medical history and monitoring the condition of patients remotely are some of the key advancements in the medical field. To improve the health of the people and to recommend the correct treatment, the correct diagnosis of disease is required. Early detection of the disease helps to cure the disease in the initial stage or makes it possible that the proper treatment is carried out. Several devices from a simple thermometer to complex electromagnetic devices are in operation in the medical sector.

The radiology technique used to detect and diagnose different diseases and injuries is the overwhelming demand of today's world. There is often a need to picture the internal body tissues/organs in case of an accident or other diseases. To understand the degree of injury one can decide when and what kind of treatment is recommended for it. Though the X-ray devices help to diagnose internal injuries, the radiations from these devices are harmful to the patients subjected to them. Moreover, during diagnosis, human bodies are exposed to various radiations, which are harmful not only to the patients but also for the workers operating those devices. To address this problem, magnetic resonance imaging (MRI) devices have been built which are free of any harmful radiation and provide better accuracy than X-ray devices. MRI devices use radio frequency signals to take the images of the internal structure of human body, providing a safe diagnostic method.

Three kinds of magnetic fields are generated in an MRI device, which are used to capture the images of internal body parts. These three types include the main magnetic field (B_o), radiofrequency field (B_1) and gradient field (B_2) (Jie, Qin, Ying & Gengying 2005). The main magnetic field is the most crucial in designing of an MRI device. The accuracy of the images depend on the strength of the main magnetic field. A very strong and uniform magnetic field (B_o) is required to capture the high quality images. The MRI devices are categorized based on the source of the main magnetic field. Different techniques are implemented to generate the main magnetic field. These techniques include superconducting magnets, electromagnets and permanent magnets to produce a uniform magnetic field in the imaging region (Trequattrini, Coscia & Pittaluga 2000). Electromagnets based MRI devices are becoming obsolete nowadays due to the very large current required to generate the main magnetic field. These devices require very thick wire with a proper cooling system. To overcome the issues faced in the electromagnets based devices, superconductive magnets were introduced which are made up of special kind of superconductive material. To bring the superconductive material in its superconducting state, cryogens are used. In superconducting state, the superconductive material offers almost zero resistance to

the flow of current (Onnes 1911). A highly uniform and strong magnetic field with less power consumption can be achieved by using this approach. They are common nowadays due to their high quality images. The only drawback of these kind of magnets is that they are expensive to build and operate. Moreover, the users need special training to handle these kind of magnets (Tadic & Fallone 2010).

Currently, the MRI devices that are employed in hospitals are heavy and difficult to relocate. To solve this problem, the author performed the modelling and design of a low cost mobile MRI device, which can be prototyped in future. The proposed MRI device can be installed in a mobile van or battlefield hospitals enabling a quick detection of injury to take necessary measures for surgery. The mobile MRI device is low cost and easy to handle. Due to its compact size it can be easily used to diagnose the disease/injury at the place of incident. Therefore, the mobile MRI units can be accessed in remote places where regular MRI facilities are not available. Moreover, it can be used in case of a natural disaster or in battlefields. In such situations, the sensitivity of the imaging is not crucial. Therefore, even the low field produced by the permanent magnets is enough to detect the internal injuries in case of an emergency. The permanent magnets are used to generate the main magnetic field for an MRI device, which are cost effective, very easy to handle, build and operate. However, the permanent magnets produce a non-uniform magnetic field. The homogeneity of these kind of magnets can be improved by optimizing the shape of the pole pieces and by implementing different shimming techniques. This thesis deals with the designing of the magnet assembly of an MRI device with improved performance.

1.1 Objectives of thesis

This thesis explores the method to design a magnet assembly for an MRI device and optimize the pole pieces shape to produce a uniform magnetic field in the imaging area. The magnet assembly design is illustrated in Fig. 1.

The objectives of this thesis are as follows,

- Design the magnet assembly of an MRI device using finite element software and analyze the magnetic field in the measuring area between the pole pieces. Calculating the homogeneity of the magnetic field in the measuring area.
- Optimize the pole pieces shape to achieve a uniform field in the diameter of spherical volume (DSV). The uniform magnetic field of 20mT in a 35cm DSV is required, which is achieved by optimizing the poles.
- Design the optimized magnet assembly in 3-D and calculating the homogeneity of the magnetic field in the measuring area.
- Design the mechanical structure of the magnet assembly to support the heavy poles and magnets.

  To achieve these objectives, a literature study is carried out. Next a 2D and 3D

models of the magnet assembly are constructed. The design is then optimized.

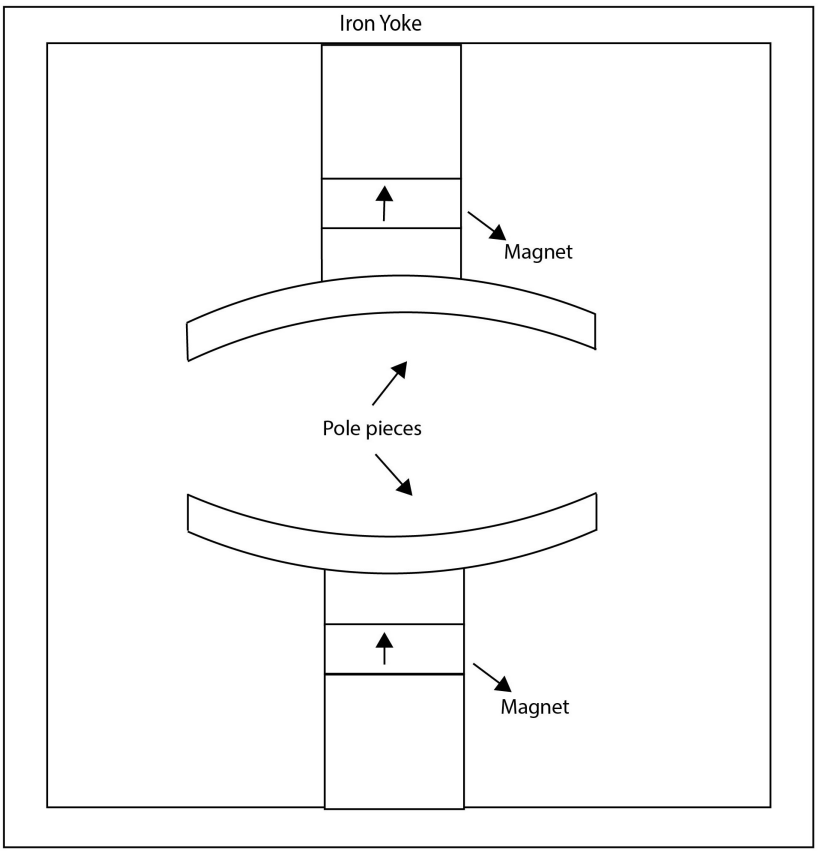

Fig. 1. 2-D illustration of the magnet assembly.

1.2 Thesis structure

This thesis is divided into five chapters. In the first chapter, a basic introduction to the topic is presented. The primary objective of the thesis with some background information is discussed. In the second chapter, a literature review is given. In the first section of this chapter, the working principles of the MRI device and its types are discussed. In the second section of this chapter, the optimization techniques are introduced briefly. In the third chapter of this thesis, a methodology for carrying out the optimization is discussed. In the first section of this chapter, the software used for the optimization is presented and the mechanical structure design is given in the end of this chapter. The fourth chapter of this thesis deals with the simulation results where the results of two and three dimensional electromagnetic and mechanical analysis are discussed. The last chapter deals with the conclusion drawn based on the simulation results.

Chapter 2

2 Background and theory

This chapter is focused on the fundamentals of an MRI device. The working principles of the device, different topologies and different methods to improve the uniformity of the magnetic field are introduced briefly. The magnet used in the assembly design and the software used for the optimization is discussed in detail.

2.1 Magnetic resonance imaging

MRI is a radiological examination technique. The MRI device constitutes of a computer interlinked with a radio frequency coils generating radio waves, and strong magnetic field source to view and generate images of the soft tissue structures (Miyamoto, Sakurai, Takabayashi & Aoki 1990). A variety of medical conditions can be diagnosed with the help of this device e.g. bones fractures, heart, chest, tumours, muscles. It's a non-ionizing device, using radio waves to capture images, so it does not emit any harmful radiations.

Three kinds of magnetic fields are generated in an MRI device which are used to generate an image. These three types include the main magnetic field B_0, radiofrequency field B_1 and gradient field B_2. A strong magnetic field B_o is produced in the imaging region to align the spin of the nuclei of the object under consideration. Once the nuclei are aligned under the effect of the applied field, a radio frequency coil is used to generate the radio frequency wave which creates a varying magnetic field (B_1). The energy applied is absorbed by these nuclei and they move to high energy states under the effect of that field. Once the application of the radio frequency waves is stopped, they come back to their original state while releasing the already absorbed energy (Haris Perlman 1993). The rate at which nuclei attain their earlier position is different due to the different tissue structures, which helps the system to distinguish between various body tissues. This process of coming back to their original state is called precession. The released energy is received by the same radio frequency coil which converts it to an electrical signal and is used to generate an image after further processing. The absorption and emission of the radio frequency field (B_1) occur at a resonant frequency. This resonant frequency depends on the strength of the main magnetic field. The gradient coils are used to create the gradient of the magnetic field, by increasing the strength of magnetic field in certain parts of the imaging region. The area with higher magnetic field strength (B_o) will require high resonant frequency to absorb the radio frequency energy. Thus, the gradient field (B_2) helps to image the human body in sections by creating an overall gradient of the magnetic field in the imaging region. The gradient field is adjusted by increasing or decreasing the amount of current flowing through the gradient coils (Anderson 1961). The operation principle of MRI device is illustrated in Fig. 2.

Different kind of MRI techniques exist depending on the kind of disease which needs to be detected. Functional MRI device and diffusion MRI device are the most common one. The diffusion MRI device takes into account the diffusion of water molecules in body tissues to generate the images. On the other hand, the functional MRI device takes into account the blood oxygenation and measure the change in the blood flow due to the brain activities. A functional MRI device is used to detect the brain injury and analyze the working of different parts of the brain relying on the amount of blood flow through them. A tumour prevents the diffusion of the water molecules within the body tissues which can be detected with the help of a diffusion MRI. The main component of an MRI device is the magnet which produces the main magnetic field (B_o) in the imaging region. Different methods and techniques are employed to produce the main magnetic field. The magnets of the MRI device are classified on the following basis, which are listed below.

1) Means by which they produce the main magnetic field.

2) Shape of the magnets, whether they are open or close.

3) Flux return path (Yoke).

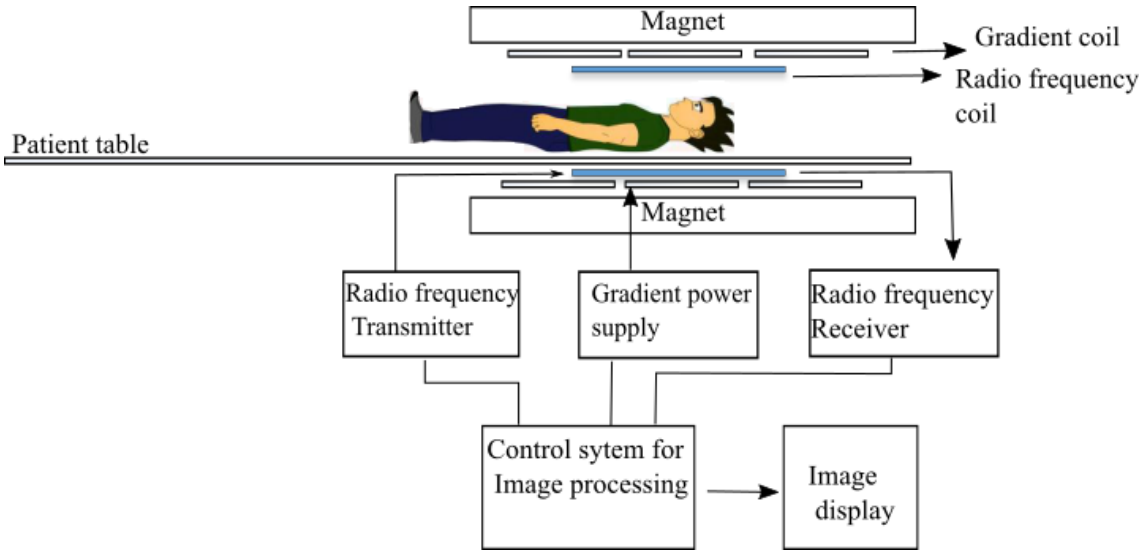

Fig. 2. Flow diagram of MRI device.

2.2 Types of MRI magnets

Three types of magnets can be used to generate the main magnetic field. These three kind of magnets are superconductive magnets, resistive magnets and permanent magnets. These three types of magnets are shown in Fig. 3 and are explained below.

2.2.1 Super conductive magnets

High field homogeneity with a field strength more than 2T can be achieved by using superconducting magnets (Molfino et al. 1988). Superconductive material usually niobium alloy is used to conduct the current. These conductors operate at a low temperature of around -270° C offering almost zero electrical resistance to the flow of the current. To achieve this extreme low temperature, liquid helium or nitrogen are used as a coolant for these conductors. Very fast and high-quality imaging can be achieved with the help of the superconductive magnets (Miyamoto et al. 1989). They are expensive due to the high capital and maintenance cost.

2.2.2 Resistive magnets

Resistive magnets are limited to the MRI applications with the magnetic field strength up to 0.5T. In resistive electromagnets, the copper conductors in the form of solenoids, coils, which carry high current are used to produce the magnetic field. These conductors offer high resistance to the flow of the current, resulting in an excess amount of heat generation. A proper cooling system (chillers) is needed to compensate for the temperature rise. This kind of magnets are less common due to their high-power consumption and cooling system requirements.

2.2.3 Permanent magnets

In permanent magnet MRI devices, the main magnetic field is produced by permanent magnet materials, usually Neodymium Iron Boron (NdFeB). They are used for medium field MRI applications producing magnetic field strength between 0.1-0.3T (Tadic & Fallone 2011). Due to the low uniformity and low field strength, these devices are not recommended where faster scanning and superior quality images are required. They are more affected by the change in temperatures, so the temperature of the room where these magnets are installed needs to be maintained at an appropriate level. The main advantage of using the permanent magnets is their smaller size and low operation cost.

A high field homogeneity is the essence of an MRI device. Unconventional permanent magnet assemblies are not able to produce the uniform field. The shape of the pole pieces need to be suitably designed in order to reach the goal of a uniform field. For the initial improvement of magnetic field uniformity, different optimization techniques are used to optimize the pole piece face of the permanent magnet MRI devices. After optimizing the pole surface, shimming schemes are implemented to further increase the uniformity. Details of shimming are given in section 2.4.

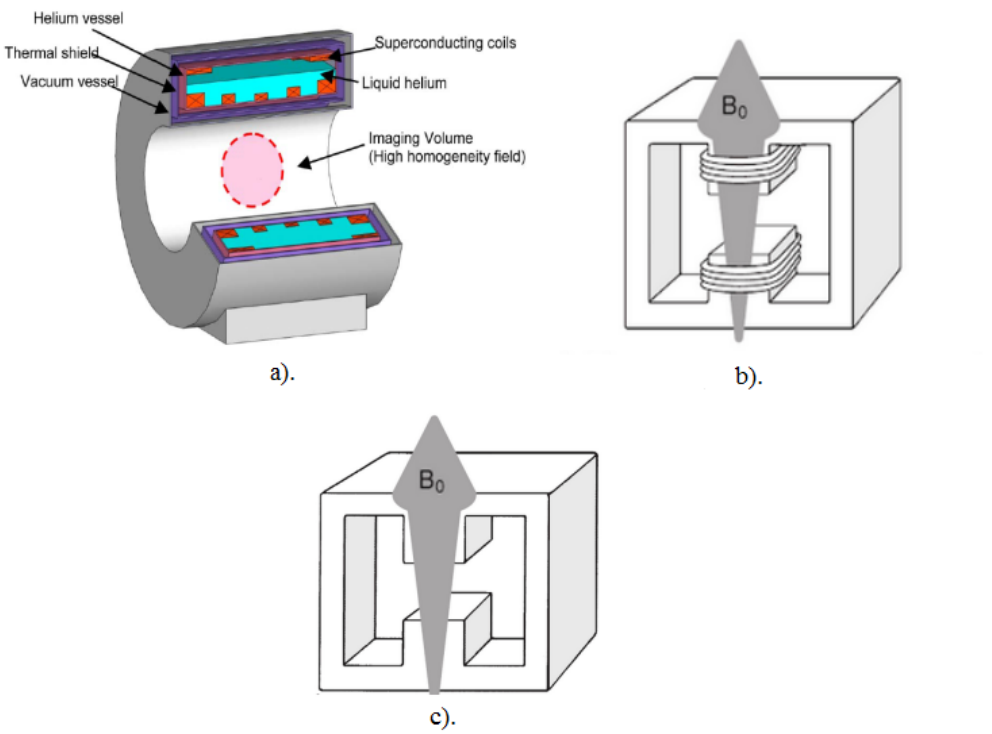

Fig. 3. Three types of MRI magnets. a). Superconductive magnet (Yamamoto et al. 2014). b). Electromagnet (Bushong & Clarke 2014). c). Permanent magnet.

2.3 Homogeneity

The homogeneity is referred to the uniformity of the magnetic field. The homogeneity is normally measured in parts per million. If we compare the magnetic field of any two points from a given diameter spherical volume (DSV), their magnetic field strength must not differ more than the said homogeneity for that DSV. The homogeneity of the magnetic field in the measuring area can be described by the following relation (Podol'Skii 2000).

$$\text{Homogeneity} = \frac{B_{\max} - B_{\min}}{B_{\text{avg}}} \times 10^6 \tag{1}$$

where $B_{\max}$ is the maximum, $B_{\min}$ is the minimum and B_{avg} is the average magnetic field intensities in the given DSV. For an MRI device, a few parts per million (PPM) homogeneity is needed, as the quality of the images directly depends on the field intensity and homogeneity in the measuring area. The desired homogeneity for these devices can be achieved by implementing different magnetic field correction methods.

2.4 Shimming

A high field uniformity in a large DSV is the basic requirement of every MRI devices. Different methods are used to maximize the uniform field in the required area of interest. Shimming is a process which increases the uniformity of the magnetic field. Shimming methods are usually employed to account for the inhomogeneities after the patient accesses the device (Xin et al. 2010).

Shimming is divided into two types, which are active and passive shimming. The strength of the magnetic field is measured along the x, y and z axis. In the active shimming method, different coils are often employed for the correction of the inhomogeneities in x, y, z, xy, yz, xz, x^2, y^2, z^2, z^3, z^4 directions (Frollo & Strolka 2001). These directions are illustrated in Fig. 5. The coils used for the correction of inhomogeneties are also known as the correction coils. The magnetic field strength is increased or decreased by adjusting the amount of current flowing through these coils. High accuracy is needed while adjusting the values of current in each coil to create a uniform field. High power consumption is a drawback of active shimming. A less expensive but a complex approach with no power consumption is the passive shimming technique, in which a ferromagnetic material (shims) are placed on the pole surface to compensate for the inhomogeneity. The passive shimming technique may include placement of several shims on the pole surface or a single ring shaped projection (Tadic & Fallone 2011). The magnetic field gradient is measured and according to it the thickness of the shim can be decided along with its orientation. Shims are applied on the pole surface, to aid the magnetic field at some point while decreasing at other. The positive shims are used to increase the magnetic field strength while the negative shims (Shims with opposite polarity of B_o) are used to reduce the magnetic field strength (Yanli et al. 2003). Yanli et al. presented the distribution of passive shims on the surface of a polepiece, which is presented in Fig. 4. Zhang proposed an integral equation method through which the effect of the magnetic field is analyzed. Based on the results, the magnetic dipoles can be placed at proper orientation to create a homogeneous magnetic field (Zhang; 1992).

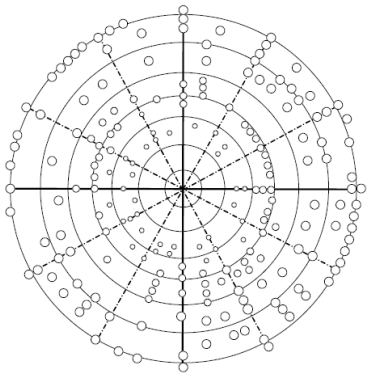

Fig. 4. Sketch map of passive shimming (Yanli et al. 2003)

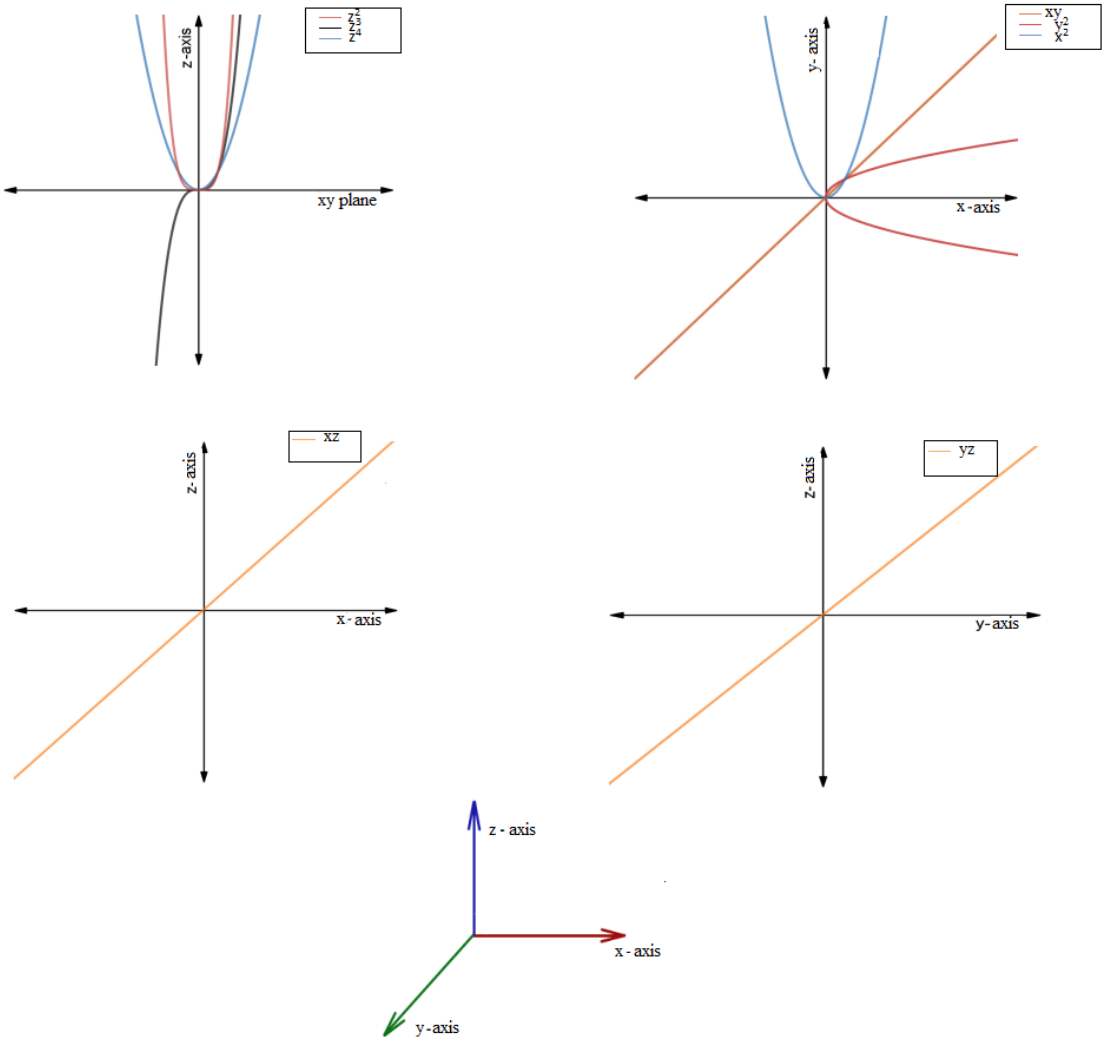

Fig. 5. Axis directions for shimming

The ferromagnetic material that is selected for the project is Neodymium Boron Iron alloy, whose details are given in section 2.5.

2.5 Neodymium iron boron (NdFeB) magnet

The magnetic materials which retain their magnetic properties even after the removal of the applied magnetic field are known as permanent magnet materials. NdFeB is the permanent magnet material which is widely used in many applications. It was developed in 1983 by Sumitomo special metals co. ltd and due to its excellent magnetic properties, this is the most suitable material to be used for an MRI device (Miyamoto, Sakurai, Takabayashi & Aoki 1989). NdFeB alloy is used as a permanent magnet material due to the high remanent flux density and the high coercive field. The NdFeB magnet belongs to the rare earth metals with a high temperature coefficient and a low curie temperature of 310° C. Due to the low curie temperature, the magnetic properties of NdFeB changes with the change in temperature. Thus, a proper temperature control system is required where these magnets are installed to keep them functioning properly.

NdFeB magnet changes its magnetic properties with the passage of time. It is reported that the flux loss of these magnets is equal to 0.07% over a 10 years period (Miyamoto, Sakurai, Takabayashi & Aoki 1989). Hence, the magnetic field strength of these magnets decreases with the passage of time which should be taken into account along with the temperature effect. These rare earth magnets are common due to their small size, low cost, high mechanical strength and energy density. The demagnetization curves of NdFeB magnets at different temperatures as given by neorem magnets oy for neorem 880a are shown in Fig. 6. The Properties of NdFeB magnets for the same grade given by neorem magnets oy are presented in Table. 1.

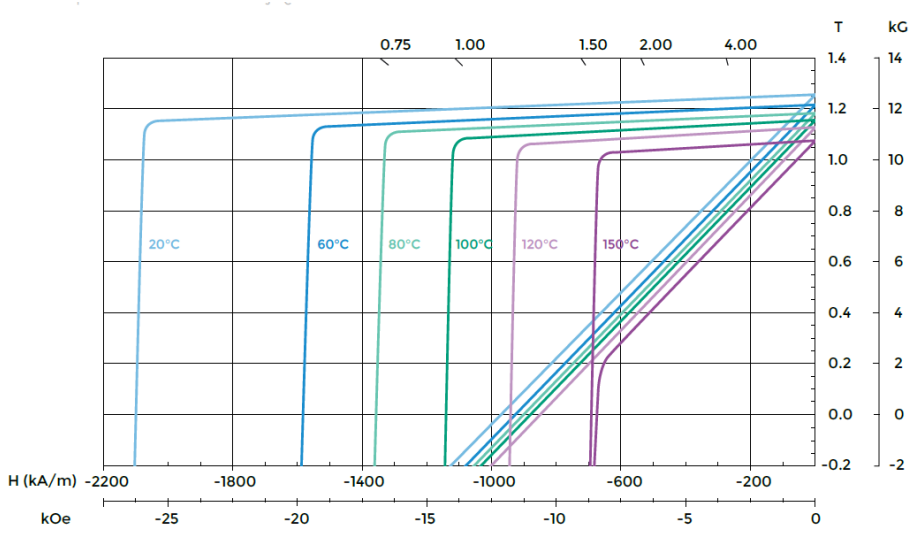

Fig. 6. Demagnetization curves of NdFeB

Magnetization characteristics of NdFeB magnets are greatly influenced when they are subjected to the change in temperature. As shown in Fig. 6, due to the increase in the operating temperature the magnetic properties of NdFeB magnet are deteriorated. The magnetic field strength of permanent magnets is inversely proportional to the temperature. As shown in Fig. 7, the remanent flux density of NdFeB magnet is decreased with the rise in temperature. These magnets are usually kept at room temperature to keep them stable.

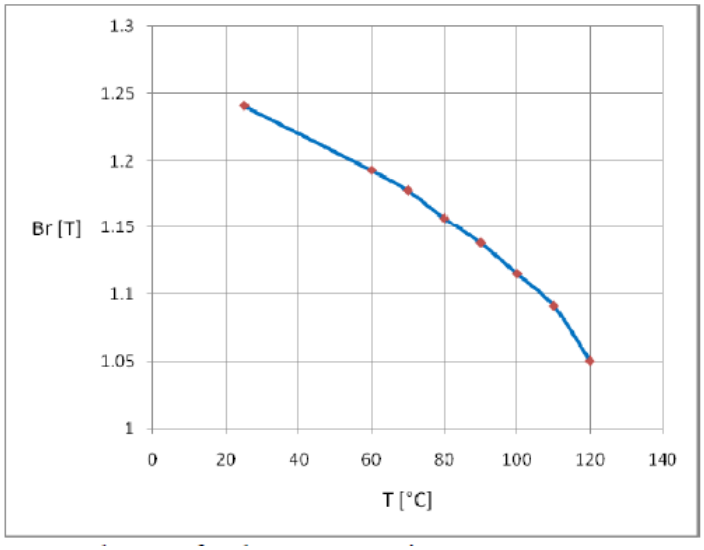

Fig. 7. Remanence flux density (Calin & Helerea 2011). (Published with permission)

The ferrite magnets are cheaper than NdFeB but they are too heavy to be feasible for an MRI device. Due to the smaller size and strong magnetization characteristics, NdFeB is the most suitable magnetic material for MRI applications. However, due to the temperature effect and surrounding objects, these magnets produce a non-uniform magnetic field (Ren et al. 2009). Thus, iron poles are used to shape the field.

Table 1: Properties of NdFeB magnet (Neorem 880a)

Material	B_r(T)	$H_c(H_{cb})$	$H_{ci}(H_{cj})$	BH_{max}	T_c	Density (ρ)
NdFeB	1.26 T	960 KA/m	2100 KA/m	300 KJ/m^3	310° C	7.6 g/cm^3

2.6 Non uniform rational b spline (NURBs)

NURBs stands for non-uniform rational B spline. It is a parametric curve which is used to draw complex designs, shapes and curves in computer aided design software. NURBs present the mathematical form of various designs and shapes. They are used to represent both analytical and free form shapes (Piegl 1991). For the construction of the curve certain control points are defined which represents the shape of the curve. Knot vector and weights are introduced which decides how close the curve will pass to the corresponding control point. By using this kind of modelling, we are able to alter a small portion of the curve without affecting the shape of the whole curve. Furthermore, it allows the user to generate a totally different curve by changing the parameters of the curve. The basic equation of NURBs curve is given as (Yuan et al. 2017).

$$S(u) = \frac{\sum_{i=1} b_i w_i N_{i,k}(u)}{N N_{i,k}(u)} for\ a \leq u \leq b \tag{2}$$

Where w_i and b_i are the weight and location of the i_{th} control point respectively. $N_{i,k}$ is the basis function occurring recursively, given as,

$$N_{i,k}(u) = \left(\frac{u - x_i}{x_{i+k-1} - x_i}\right) N_{i,k-1}(u) + \left(\frac{x_{i+k} - u}{x_{i+k} - x_{i+k}} N_{i+1,k-1}(u)\right) \tag{3}$$

$$N_{i,0}(u) = \begin{pmatrix} 1 & x_i \leq u \leq x_{i+1} \\ 0 & otherwise \end{pmatrix} \tag{4}$$

where k is the order of the curve, N is the b spline basic function and $\boldsymbol{x} = [x_1..x_N]^T$ is the knot vector. The order of the curve, knot vector, weight and control points are the basic components for the construction of NURBs curve. The order of the curve depends on the curve if it is linear, quadratic or cubic. The effect of the order on the shape of the curve is shown in Albert technical memo, which is presented in Fig. 8 (Peterson 1990). The control points which define the shape of NURBs curve should be equal to or greater than the order of the curve. Certain weights are assigned to each of the control points. The weights decide how closely a line will pass from a control point. The curve will pass through that particular control point which is assigned the maximum weight. Equal weights are assigned to all the control points, irrespective of the value of weights, to make the curve non-rational. Another parameter that affects the shape of the curve is the knot vector. The knot vector values are altered to modify the shape of a curve (Liu 2003). They can make a curve smoother or irregular and are used to break the parametric space into the knot spans. The knots are always allocated values in ascending order. The number of knots is calculated by the following formula (Fazanaro et al. 2016).

$$k = cp + d + 1 \tag{5}$$

where k is the number of knots, cp is the number of control points defining the curve and d is the degree of curve.

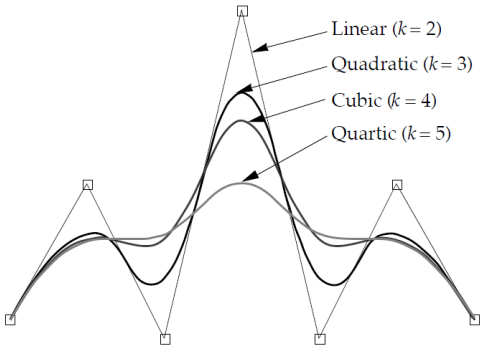

Fig. 8. Curve order (Peterson 1990).

The pinned uniform knot vectors are implemented to force the curve to pass through the first and last control point. The pinned curve will not go through the other control points between the endpoints, it will only pass near to the other control points depending upon the value of weight (Peterson 1990). In Fig. 9, the unpinned curve cannot reach the endpoints, as it only passes close to all the points between the endpoints without touching them.

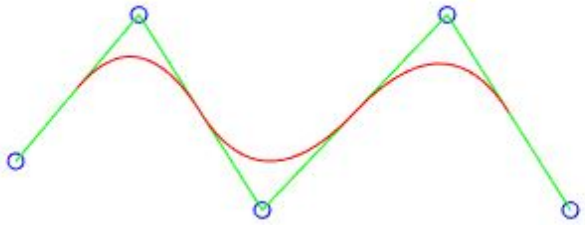

Fig. 9. Unpinned Curve

Matlab's mathematical toolbox NURBs can be utilized to control the shape of the pole piece in the optimization algorithm. The faces of the upper and lower pole pieces are implemented with NURBs function, to get the shape that can result in a maximum magnetic field in the imaging area. As shown in Fig. 10, the faces of lower and upper poles are drawn by NURBs curve, which provides the flexibility of altering the face of the pole.

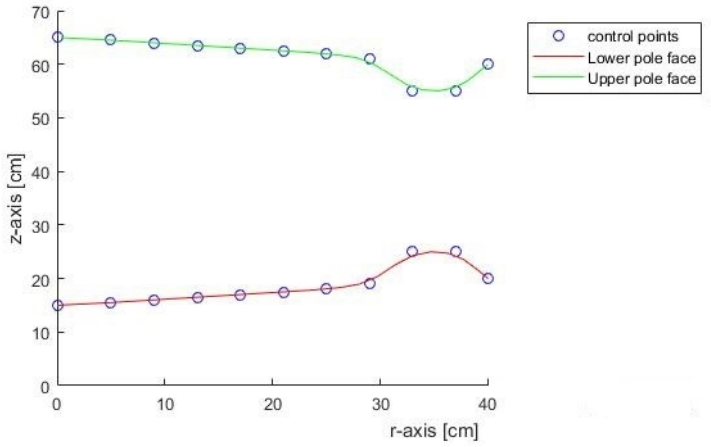

Fig. 10. NURBS curve for pole face

2.7 Optimization techniques

Complicated problems that are difficult to solve analytically can be optimized to get the best possible result. An objective function needs to be defined which can be evaluated for its maximum or minimum value depending upon the requirement. Different optimization algorithms like genetic algorithms (G.A), tabu search scheme, particle swarm optimization algorithm (PSO) iteratively solve the complex problems searching for the best possible solution.

Holland (1975) has developed G.A for the optimization of complex problems. In G.A, all parameters are transformed into binary strings. Selection, mutation and crossover of the individuals is carried out to get the best solution. Cheng et al. (2013) used a G.A for optimizing the shimming ring of polepiece for an MRI device. By optimizing the shimming ring the magnetic field uniformity is increased by 65 percent than without shimming rings.

Glover (1986) introduced the tabu search scheme to solve the optimization problems. Tabu search introduces a meta-heuristic approach to investigate all parts of a search space. It forces the investigating procedure to always transform from one solution to another in a quest of getting the global optimal solution. An attribute based memory concept is introduced in this algorithm, which keeps the record of every solution and a step through which that solution is generated (Leonard & Connor 2000). Every possible move can either result in an improved or a deteriorated solution. The result of each progressive step is saved. As a result, the already visited solutions are skipped and there is more probability of finding the better solutions by investigating the unknown parts of the search space resulting in the improved performance. This strategy of exploring the newer parts of the search space is called diversification. Leonard used the tabu search scheme to optimize the shape of the pole piece. Several pole shapes were generated by using different parametrizations in tabu search algorithm (Leonard & Connor 2000).

PSO is an efficient algorithm to solve optimization problems, Cheng et. al, used PSO to optimize the shape of a shimming ring for permanent magnet MRI device (Cheng et al. 2012). By using PSO they improved the uniformity of magnetic field by 66 percent. This algorithm can be used to optimize nonlinear functions. It is very simple and can be implemented for any type of problem.

2.8 Particle swarm optimization

Kennedy & Eberhart (1995) developed a swarm based intelligent algorithm which can be used to optimize a wide variety of functions. They have developed the idea from the flock of birds, based on how they move in the form of flocks with each other in the search for food. Birds are called particles and food is the target or objective function in this algorithm. The birds are initially not aware of the location of the food, but as they move they keep on updating each other about their best position to reach their target. The idea of this internal communication to update each other about their best position and velocity resulted in the development of an optimization algorithm named as particle swarm optimization algorithm.

The PSO algorithm is used to find the minimum or maximum of a function by updating the position and the velocity of the particles in each iteration. The advantage of using PSO is that no previous knowledge of the position of the particles and type of objective function is required (Blondin 2009). It initializes the particles (parameters) with some random values and evaluates them for a given fitness function resulting in a fitness value of each individual particle. Initialization of the candidate solutions is always subjected to certain constraints so that they confide in the solution region. The evaluated fitness values are then compared, and subsequently, the best fitness value is saved and is named as particles best value (pbest). Another best fitness value attained by the particles within its neighbouring particles/candidate solutions is calculated and stored, which is named as global best (gbest). In each iteration, these values are updated if better gbest and pbest are found, and it keeps the previous ones if they are better than the newly calculated values. The velocity and position of the particles are updated in each iteration based on the best particles position and velocity. Thus, by tracking and updating the record of the position and velocity of the best particles, in each iteration, the optimization algorithm moves closer to the final solution. The optimization algorithm is easy to use as it only requires few parameters, constraints and an objective function. The stopping criteria for the algorithm is defined based on the convergence of the algorithm or the maximum number of iterations. The algorithm keeps on iterating until the maximum number of iterations is reached or the best solution is found (Zitzler et al. 2004). The particles position and velocity for PSO can be written as (Blondin 2009):

$$V_i(t+1) = w * V_i(t) + C_1 r_1[\hat{x}_i(t) - x_i(t)] + C_2 r_2[g(t) - x_i(t)] \tag{6}$$

Each particles position is updated as.

$$x_i(t+1) = x_i(t) + v_i(t+1) \tag{7}$$

where i is the index of each particle. v and x are the velocity and the position of i_{th} particle at time t respectively. $\hat{x}_i(t)$ is the particle's best value while g(t) is the global best value at time t (Blondin 2009). r_1 and r_2 are random values which are reproduced every time while calculating the new velocity value. These random coefficients are used to mimic the stochastic nature of the swarm. These two randomly generated numbers r_1 and r_2 corresponds to two separate calls to the function and are varied uniformly between 0 and 1 (Robinson & Rahmat-Samii 2004). Hence, the relative pull of pbest and gbest vary between 0 and 1. $w^*V_i(t)$ is the inertial weight which forces the particle to move in the desired direction. Its value is in the range between 0.9-0.4 (Shi & Eberhart 1999). The large inertial weight forces the particles to move towards their global best solution while the low inertial weight facilitates a local search. In the algorithm, generally a large value is allocated to the inertial weight which is decreased linearly during the course of the optimization process. Hence, the algorithm has more global search ability in the start while near the end of the optimization process, it has more local search ability (Shi & Eberhart 1999). The inertial weight is defined as 0.9 and is decreased linearly to 0.4 for better results. C_1 and C_2 are the acceleration coefficients, which shows the convergence rate of the algorithm towards the individual best solution and global best solution respectively. C_1 and C_2 are normally allocated values close to 2. The basic steps of PSO algorithm are represented by a simple flow diagram shown in Fig. 11.

2.8.1 Population size

Swarm size or population size is usually between 20-30. In the initialization of the algorithm, candidate solutions are randomly generated within a search space and during each iteration, the best result is saved. If the swarm size is 25, it means that 25 different candidate solutions (particles) are generated as an input to the fitness function and the one with the best fitness value is saved for the next iteration. If the swarm size is low, then it is possible that the algorithm will converge to a local minimum. On the contrary, if the swarm size is too high then it may increase the computation time. Thus, we have selected 25 as the approximately optimal swarm size for the optimization of the pole surface.

2.8.2 Number of iterations

The number of iterations defines how many times the candidate solution is generated for the evaluation of the objective function. The stop criterion for the algorithm can be defined as the maximum number of iterations or it can be based on the relative improvement of the candidate solution. If there is no substantial change in a

candidate solution for last 20 iterations then the algorithm will attain its convergence criteria. In this work, when the difference between the last iteration result and the 20th last iteration is less than 1e-6, the algorithm is converged. We computed the algorithm for 1000 iterations, every time the algorithm is converged to the optimal solution after 400-500 iterations as per aforementioned criteria. In each iteration of the optimization algorithm, the axisymmetric finite element model of the magnet assembly is built for each particle.

2.8.3 Boundary limits

The search space (solution region) is defined by the maximum and minimum boundary limits. Boundary limits make it possible for the algorithm to search for the optimal solution within the defined search space. The search space size is altered by varying the boundary limits so that the algorithm can explore different areas of the solution region. If the search space is too small then it is possible that the algorithm may not find the best result. On the contrary, if it is too large, it may find the better result after several iterations. The boundary limits for the magnet assembly model are given in chapter 3.

2.8.4 Design variables

Design variables or the decision variables are the input parameters which defines the dimension of a problem. The complexity of the optimization problem increases by increasing the number of decision variables. The decision variables are generated based on the position and velocity equations in each iteration while searching for the best solution. We tested different cases by varying the number of decision variables. The control points of the spline curve defining the pole face, dimensions of the magnet and yoke serve the purpose of the design variables in the optimization algorithm.

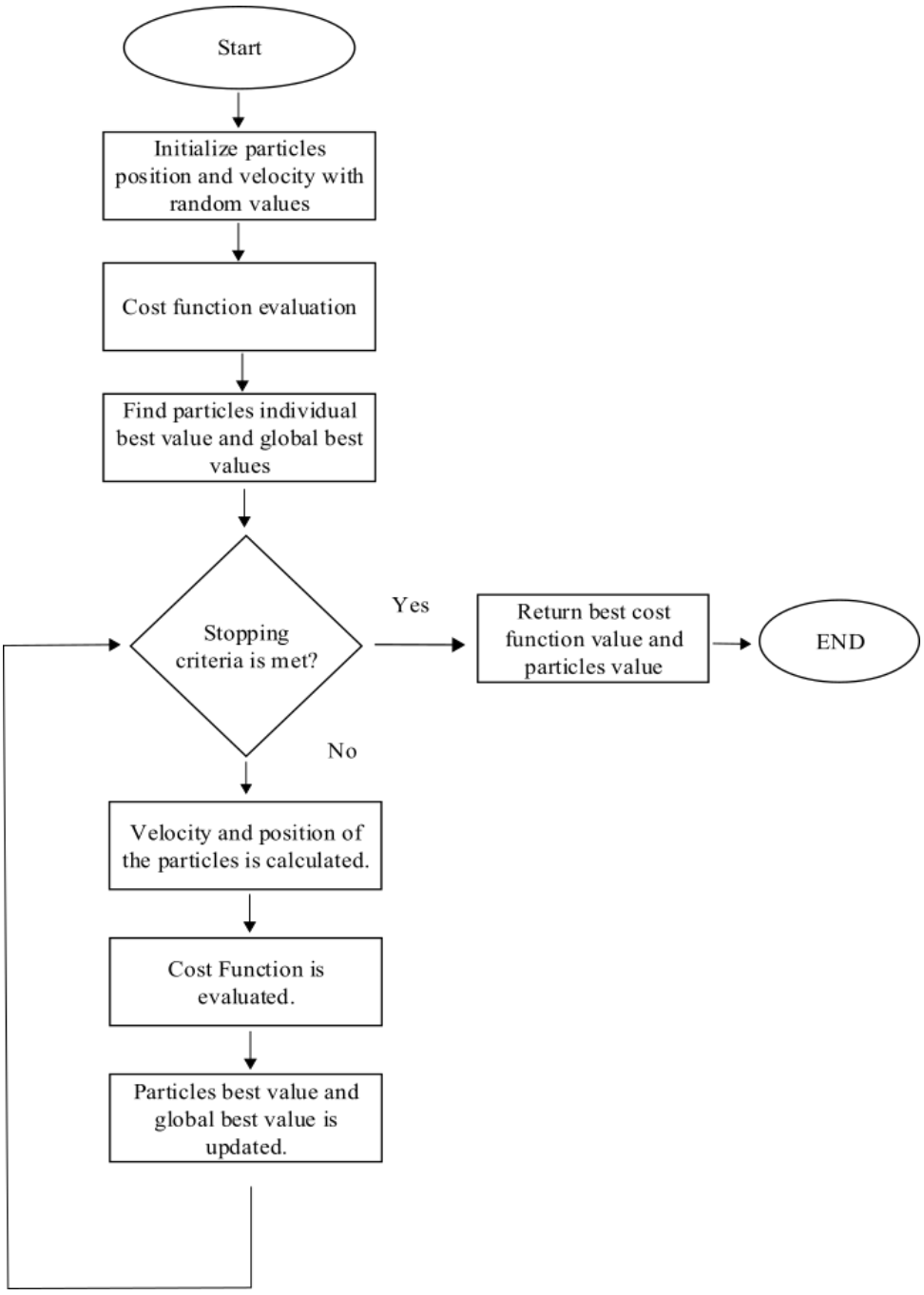

Fig. 11. PSO flow chart

Chapter 3

3 Design and optimization

In this chapter, the design and optimization methodology of the pole piece shape for the MRI device is discussed. The design of the magnet assembly is presented in the first section. In the second section, the FE method used for the 2D electromagnetic analysis is discussed. The optimization of the pole faces using PSO algorithm is discussed in the third section. In the fourth section, the method of the 3D electromechanical analysis is presented.

3.1 Design of magnet assembly

This thesis focus on the optimal design of the magnet poles for an MRI device. Initially, the 2D finite element software FEMM v4.2 is used to model an axisymmetric geometry of the magnet assembly. NdFeB magnet is selected due to its high remanent flux density to generate the magnetic field. The iron is selected as a pole-piece material due to its high permeability. NdFeB magnets are hard and brittle. Moreover, a very high accuracy is required to manufacture these magnets. Due to the manufacturing tolerances, the magnets shape affects the performance of these magnets. Hence, they are not able to produce a uniform magnetic field in the imaging region. The pole pieces are placed on the surface of the magnets to increase the magnetic field uniformity (Cheng et al. 2015). The pole pieces are placed facing each other with a separation of 50cm. The placement of the pole pieces needs to be accurate. If the poles are tilted even by few millimetres, the magnetic field uniformity in the imaging area is disturbed. As presented in Fig. 1, the poles and magnets are supported by the mechanical structure, which needs to be stiff enough to sustain the weight of the magnet assembly.

The pole piece faces are parametrized and drawn by NURBs using Matlab's inbuilt function so that they can be optimized for improving the uniformity of the magnetic field. The selection of the parameters defining the pole surface and dimensions of the magnet assembly are crucial for the optimization problem. It is worth to remember that if there are too many parameters, then there is a possibility that the algorithm will not give an optimal result. Also in case of a low number of parameters, the optimal solution may exist out of the solution region (Leonard & Connor 2000). The geometry is designed in FEMM v4.2 by using MATLAB functions and optimized using PSO algorithm. The optimized model is built in 3D using Comsol to check the homogeneity of the magnetic field as well as the mechanical stability of the designed structure. The maximum field that is targeted in this work is 20mT. To achieve the desired magnetic field strength, the dimensions of the magnet are parametrized in the algorithm. The surface of the pole is implemented with pinned uniform b

spline curve. Thus, the diameter of the pole is fixed while the surface of the pole is parametrized. The design parameters for the MRI device are presented in Table 2.

Table 2: Design parameters

Gap length	50 cm
Field strength	20mT
Homogeneous space	35 cm DSV
Pole Piece diameter	80 cm
Permanent magnet	40 cm

3.2 Axisymmetric finite element model

3.2.1 Governing Maxwell's equations

Maxwell equations are the set of equations, which are used to define the fundamentals of electromagnetic fields, space and time relationship between electricity and magnetism.

In case there are no current distributions in the problem region, the governing equations are given as

$$\nabla.\boldsymbol{B} = 0 \tag{8}$$

$$\nabla \times \boldsymbol{H} = 0 \tag{9}$$

Since we are using permanent magnets, the magnetic flux density ($\boldsymbol{B}$) is related to the magnetic field strength ($\boldsymbol{H}$) in air by the following relation

$$\boldsymbol{B} = \mu_o(\boldsymbol{H} + \boldsymbol{M}) \tag{10}$$

where, $\boldsymbol{M}$ is the magnetization

μ_0 is the permeability of the vacuum

3.2.2 FE method

The FE method is used to numerically solve boundary value problems that emanate from physical phenomena ruled by some spatial differential equations. The main idea of FEM is to divide the region under consideration into smaller subregions. The smaller subregions are called as finite elements. Each of the finite element represents a simple function. The simple function of each region, generally a polynomial, is solved to approximate the field solution. To increase the accuracy of the solution, the division of the region into smaller subregions can be made denser. The process of dividing the problem into smaller finite elements is called meshing. Certain points are defined within the problem region, which are called nodal points. The field values

are generally computed on these nodal points. The shape functions are chosen in such a way that each shape function corresponds to a unity value on selected node, while it is zero for all other nodes. The location and number of nodes determine the order of the shape functions. Further, the global shape function is formed by combining all the individual shape functions.

In irrotational fields, $\boldsymbol{H}$ can be modelled as a magnetic scalar potential (ψ)

$$\boldsymbol{H} = -\nabla\psi \tag{11}$$

By substituting the Eq. 10, in Eq. 8, we can get

$$\nabla.(\mu_0(\boldsymbol{H}+\boldsymbol{M})) = 0 \tag{12}$$

Now substituting the value of $\boldsymbol{H}$ in the above equation, we can get the div-grad equation as

$$\nabla(\mu_o\boldsymbol{M} - \mu_o\nabla\psi) = 0 \tag{13}$$

$$\nabla.(\nabla\psi) = \nabla.\boldsymbol{M} \tag{14}$$

The term on the right hand side of the Eq. 14, is due to the permanent magnets. In case of the permanent magnets, $\boldsymbol{H}$ is not equal to zero at $\boldsymbol{B} = 0$. The scalar potential ψ should satisfy the Maxwell's equation within our defined boundary conditions. By discretizing using FEM, the scalar potential can be approximated by the following equation

$$\psi = \sum \psi_j N_j \tag{15}$$

where N_j and ψ_j are the shape function and the nodal scalar potential of node j, respectively. The div-grad equation given in Eq. 14, is solved by using the galerkin method of weighted residuals to get a system of linear equations. The FE assembly matrix is given as

$$\boldsymbol{S\psi} = \boldsymbol{f} \tag{16}$$

where $\boldsymbol{S}$ is the stiffness matrix, $\boldsymbol{\psi}$ is an unknown vector containing the nodal values of the magnetic scalar potential and $\boldsymbol{f}$ is the source vector. The stiffness matrix $\boldsymbol{S}$ has the entries

$$\boldsymbol{S}_{ij} = \int \nabla N_i \cdot \nabla N_j dS \tag{17}$$

The source vector $\boldsymbol{f}$ has the entries

$$\boldsymbol{f}_i = \int \boldsymbol{M}\nabla N_i \tag{18}$$

Finally, the nodal values of the scalar potential are solved as

$$\boldsymbol{\psi} = \boldsymbol{S}^{-1}\boldsymbol{f} \tag{19}$$

Different numerical techniques can be used to solve the above equation depending upon the nature of the problem.

3.2.3 Magnet assembly model in FEMM

For axisymmetric problems, the problem depth is zero. Depth represents the length of the geometry into the page direction, which is defined usually for the 2D planar problems. Further, the minimum angle is defined in the problem definition. The minimum angle corresponds to the minimum angle of the triangle during meshing. By applying the constraint of minimum angle, no angle less then the specified value occurs in a mesh.

The axisymmetric geometry of magnet poles of an MRI device is designed in FEMM using OctaveFEMM. OctaveFEMM is a Matlab's toolbox used to parametrize the geometry, material properties and start the FEMM program with these parameters. The toolbox allows accessing electrostatics, magneto-statics and heat flow problems in FEMM, by providing separate command sets according to the nature of a problem. Magnetostatics pre and post-processing tools of FEMM are used to design and analyze the device model. For each boundary of the designed magnet assembly, the boundary conditions are defined, which are shown in Fig. 12. The Neumann and Dirichlet boundary conditions are given as.

$$\text{Neumann} : \mu(\boldsymbol{M} - \nabla\psi).\boldsymbol{n} = 0 \tag{20}$$

$$\text{Dirichlet} : \psi = 0 \tag{21}$$

where $\boldsymbol{\psi}$ represents the magnetic scalar potential and $\boldsymbol{n}$ is the direction normal to the surface. All the domain boundaries of the magnet assembly are defined by the neumann boundary condition except the outer boundary. The outer boundary of the magnet assembly is defined by the open boundary condition. Open boundaries are often needed to compute the field in an unbounded space, without having any effect of the nearby computational boundary. For FEM computations, the domain must be bounded to approximate a solution. To define an open boundary condition in FE software, the truncation method is usually used. In the truncation method, a larger region than the main area of interest is approximated and the magnetic scalar potential is equated to zero (ψ=0) on an arbitrary boundary that is 5 times far away from the main region (Meeker 2010). The external boundary of the designed magnet assembly is defined by using the truncation method. Due to the approximation of such a large area, the computational time is increased significantly. To reduce the computation time, a very coarse mesh is generated for the area that is external to the main region.

By using the post-processing commands of FEMM, the field values of $\boldsymbol{B}$ and $\boldsymbol{H}$ are analyzed. The magnetic field at discrete points within the DSV is calculated, which is then used to compute the homogeneity of the magnetic field in the area of interest. The axisymmetric geometry is presented in Fig. 12 and simulation parameters are shown in Table 3-4.

Table 3: Materials

Magnet	NdFeB
Pole piece	Iron
Surroundings	Air

Table 4: Problem definition

Problem Type	AxiSymmetric
Length Units	cm
Frequency	0
Depth	0
Solver Precision	1e-08
Minimum Angle	30

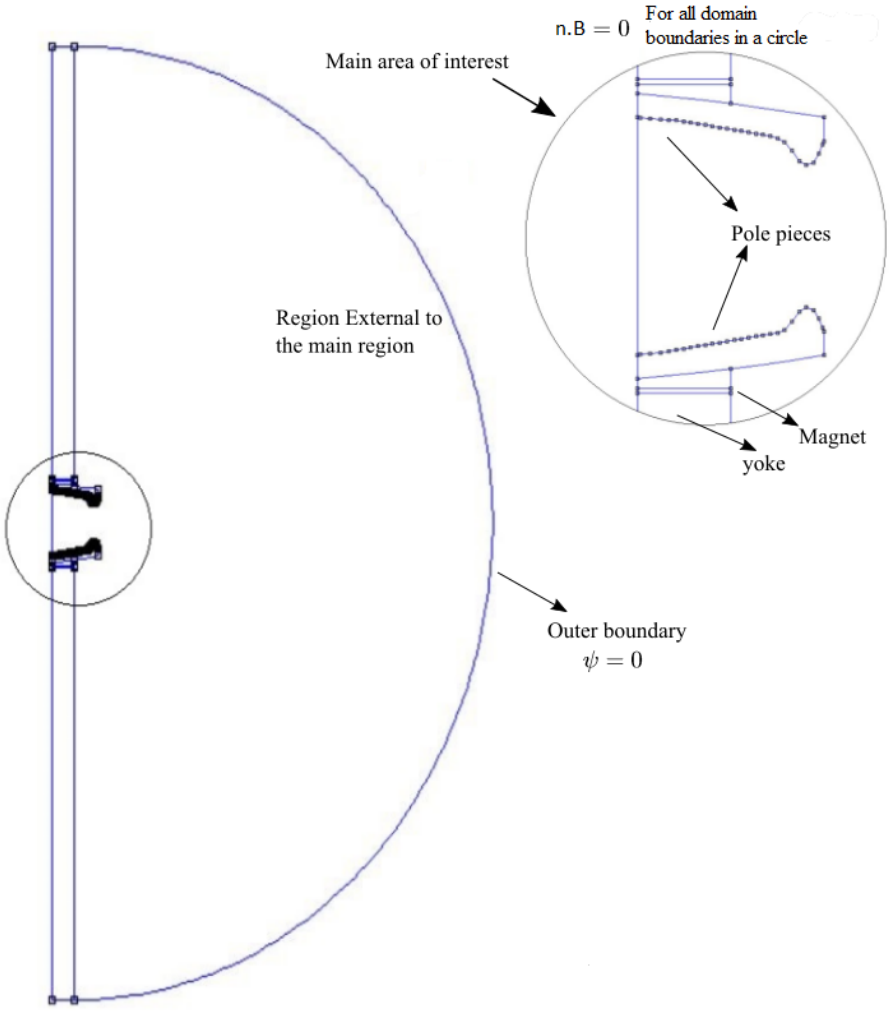

Fig. 12. Axisymmetric geometry of the magnet assembly in FEMM

3.3 Optimization method

A design of permanent magnet MRI is presented in Fig. 12. Permanent magnets are used as a source of the main magnetic field in the imaging region. The field produced by the permanent magnets is not uniform. To achieve a uniform magnetic field in the imaging region we must seek for the optimum pole piece shape. The points defining the face of the pole pieces are parametrized and NURBs curve is fitted with those points to smoothen the pole face. Increasing or decreasing the number of control points directly affects the design of the pole piece and the uniformity of the field. Thus, the polepiece face is optimized by varying the number of control points. The diameter of the pole pieces is 80cm and the imaging region of 35cm DSV is chosen. The distance between the centre of both pole pieces is fixed at 50cm.

The PSO algorithm is used to optimize the magnet assembly design. Details are presented in the next sections.

3.3.1 Particle Swarm Optimization

The PSO algorithm starts by initializing each particle by some random value, evaluates the objective function and try to minimize the objective function by improving the particles values. Particles keep on communicating with each other, updating each other which particle generated the best result during each iteration. They are confined to predefined search space and they try to move towards their own best position and swarm's best position which can generate the best fitness value.

3.3.2 Parameters of PSO

The values of parameters used by the optimization algorithm are given below. These parameters are already explained in chapter 2.

- C_1 defines the convergence rate towards local optima while C_2 defines the convergence of the algorithm towards global optima. $C_1 = C_2 = 2$.
- The number of design variables in the MRI model are 3-13.
- r_1 and r_2 are coefficients which are assigned random values in each iteration.
- w =0.9.
- Population size = 25.

3.3.3 Problem definition

For the optimization algorithm, we defined the objective function, boundary limits, stopping criteria and population size. The objective function value depends on the input definition set. Lower and upper boundaries for input definitions are defined to

restrict them within a defined set. The dimensions of magnet, yoke and parameters of the pole piece face are input to the PSO algorithm. The boundaries of the pole piece faces are arbitrarily chosen keeping in mind the distance between the poles and a maximum thickness of the pole piece. The control points defining the pole surface and the points defining the dimensions of the magnet assembly are varied within a range of ±3cm of the initial design. These boundaries define the search space for the algorithm in which it will find the candidate solution (value of a parameter) that can provide the best possible result. During each iteration, the algorithm will explore unknown parts of the search space in a quest of finding the optimal shape of the pole, which can produce a uniform magnetic field.

In the optimization algorithm, the pole faces are defined as symmetric. Instead of parametrizing both pole faces, only the lower pole piece parameters, which are the control points of the NURBS curve are provided as an input to the optimization algorithm. Thus, due to the symmetry number of design variables are reduced to half resulting in a less computation time. The first and last control point of the spline curve is forced to keep the same value in each iteration of the algorithm, so that the spline curve always passes through its first and last control point, resulting in a closed domain.

3.3.4 Objective function

The objective function is often referred to as the fitness function or cost function. The objective function is used to calculate the fitness value of each particle. The optimization algorithm minimizes the objective function in each iteration, keeping a record of the pbest and gbest. In this case, the homogeneity of the magnetic field in the imaging area between the two poles is our objective function, which is defined as.

$$\text{Homogeneity} = \frac{B_{\text{max}} - B_{\text{min}}}{B_{\text{avg}}} \times 10^6 \tag{22}$$

where B_{max} is the maximum, B_{min} is the minimum and B_{avg} is the average magnetic field intensity in the given DSV of 35cm. Eleven points equidistant from each other on the DSV are chosen on which the magnitude of the magnetic field is calculated. The calculated magnetic field values are used to compute the homogeneity of the magnetic field. As the stopping criteria is met, the algorithm will return the minimum value of the cost function and the parameters which resulted in the minimum value of the cost function.

3.4 3-D electromagnetic design in Comsol

FE method is a numerical analysis tool, which is used for the accurate field calculations. The FE software's are used for the analysis of the magnetic field. The designed magnet assembly is implemented in a commercially available software Comsol Multiphysics v5.3a, which uses FE method to solve the magnetic field problem.

The 2D FE analysis of the given magnet assembly has already been performed, which was sufficient to approximate the behaviour of the magnetic field in the measuring area. Due to the complexity of the designed assembly and to take into account all the effects that our model will be subjected to in reality, a 3D model is built. The magnet poles are designed in 2D workplane, which are revolved to get the 3D design. The same material properties that are defined in FEMM software are used in comsol simulations. The material used for the magnets is NdFeB and that for the polepieces is iron. A tetrahedral mesh is generated for our geometry and a stationary solver is chosen to study the model. The magnetic field no currents application module is selected to compute the magnetic scalar potential (ψ) at discrete points.

In Fig. 13, we present the 3D model geometry used for the FE calculations in comsol. In Fig. 14, the homogeneity of the flat pole shape is presented. It can be seen that the flat pole shape does not produce a uniform magnetic field in the imaging region. To overcome this issue of non uniformity, pole faces are optimized. The pole faces before and after optimization are modelled in comsol and results are presented in chapter 4. Further, to confirm the stability of the designed structure, the mechanical analysis is performed. The details of the mechanical analysis are given in section 3.4.1.

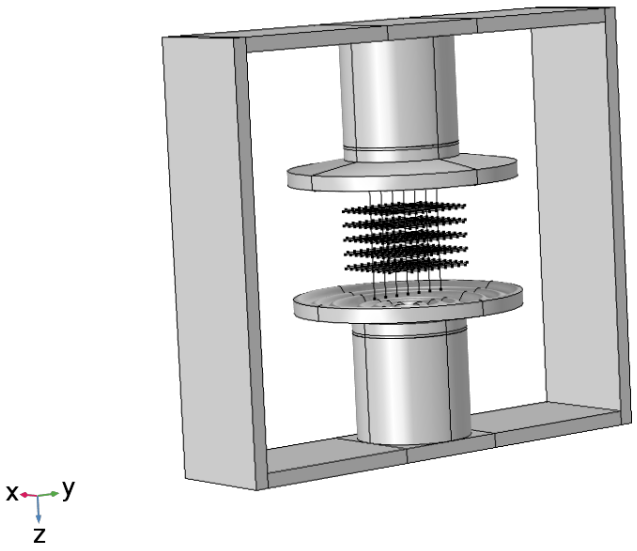

Fig. 13. 3-D geometry of designed assembly in COMSOL

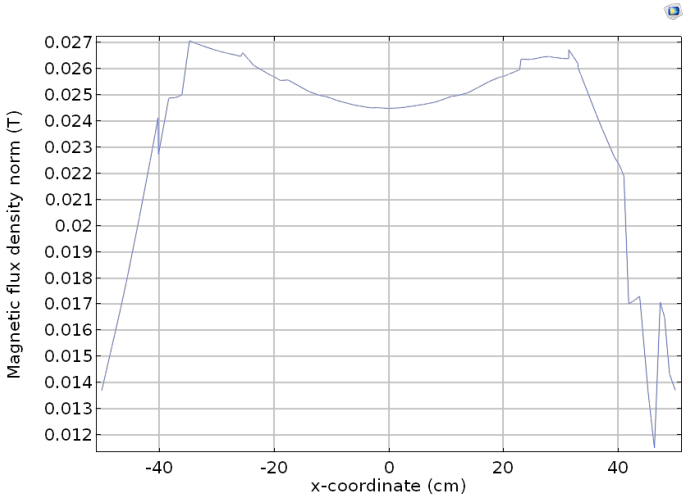

Fig. 14. Magnetic flux density in the imaging area (before optimization).

3.4.1 Mechanical structure design

The mechanical structure is required to provide support to the magnet assembly. A very high accuracy is needed while designing the mechanical structure. If the poles or the magnets are not accurately placed, they might affect the uniformity of the magnetic field. Thus, there is a need for a proper mechanical structure design that can bear the weight of the heavy pole pieces and magnets, without causing any deformation in the structure.

Three types of mechanical structures are common for permanent magnet MRI assembly design, which are four column, two column and C shape. These three types of structures are shown in Fig. 15 (Jiang et al. 2004). The mechanical structure serves mainly three purposes. Firstly, it provides mechanical support to the poles and magnets. Secondly, it provides the return path to the magnetic field. Thirdly, it limits the flux leakage by forcing the field lines to stay in the yoke. Two column mechanical structure is chosen for the magnet assembly, to provide support to the heavy poles and magnets. Additionally, it provides a wider access for the patient under examination. The dimensions of the mechanical structure holding the magnet assembly are approximated such that the flux leakage from the poles to the walls is minimal. The designed mechanical structure is shown in Fig. 16. In Fig. 16, the radial direction is represented by y-axis and the axial direction is represented by z-axis.

Due to the high magnetic permeability and high mechanical strength, iron is chosen as a material for the mechanical structure design (yoke). The material properties of iron are given in Table. 5. Solid mechanics mode of Comsol Multiphysics is used to analyze the effect of such a heavy mass on the designed model. The base of the mechanical structure is fixed to the ground; thus, it will not move. Therefore, the domains at the bottom of a mechanical structure are defined as a fixed constraint. The force equal to the mass density times gravity (force perunit volume) is applied

at each point of the magnet assembly model and simulated. The stress analysis in post-processing of comsol software is performed to check for the strength of the designed structure. The weight and dimensions of the whole assembly are calculated and are presented in the results section.

Table 5: Properties of Iron

Material	**Density**	**Poisson's ratio**	**Youngs modulus**	**Yield strength**
Iron	7.87 (g/cm^3)	0.291	200 (GPa)	50 (GPa)

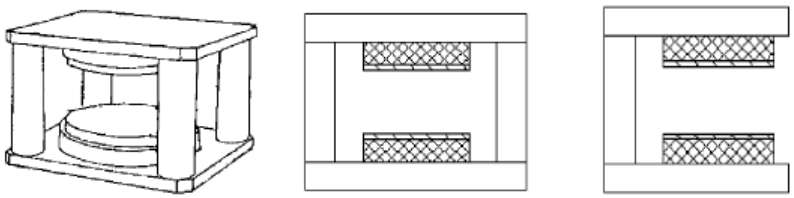

Fig. 15. Mechanical structure designs (Jiang et al. 2004). a) Four column. b). Two column. c). C shaped.

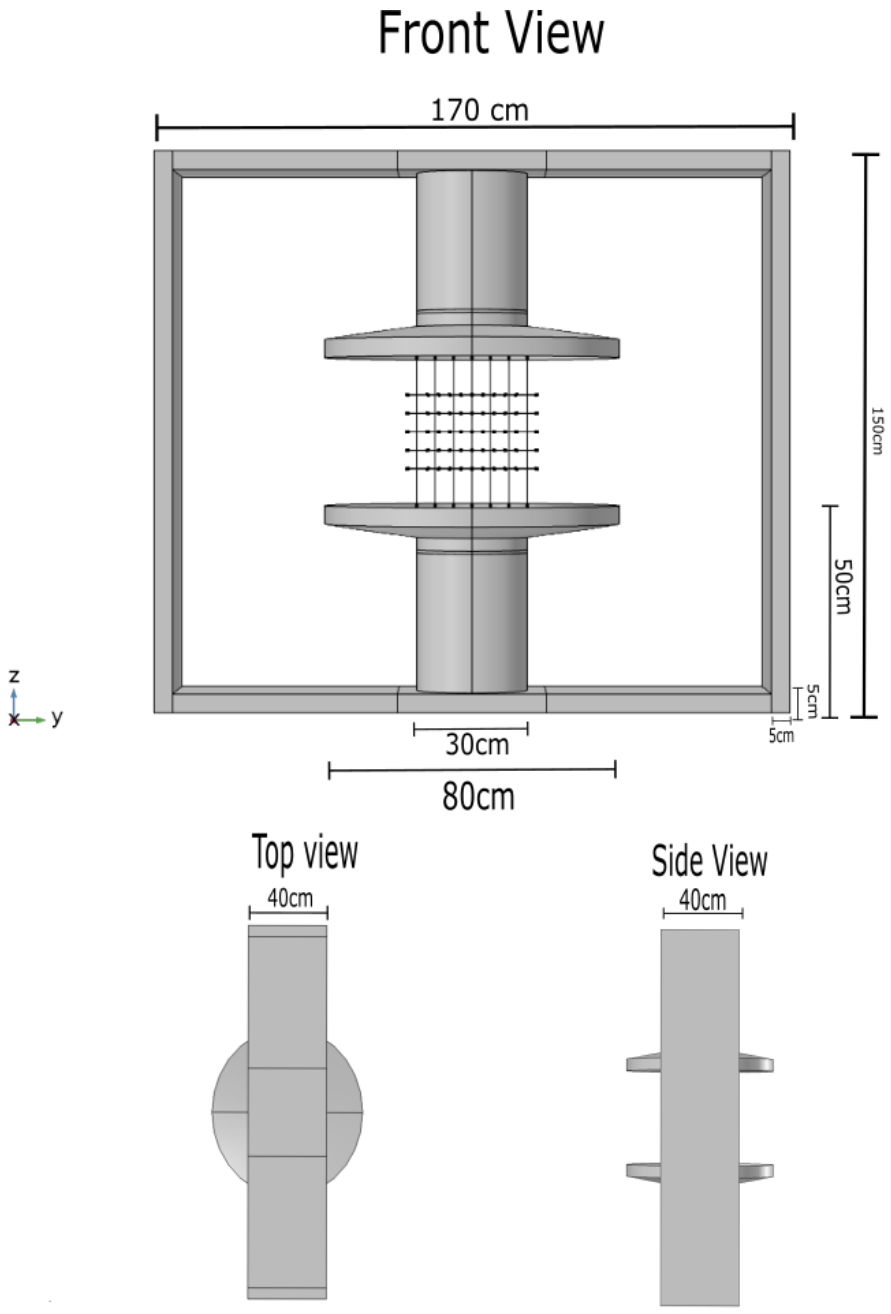

Fig. 16. Mechanical structure of designed magnet assembly

Chapter 4

4 Results and discussions

The results of this thesis are divided into three different sections. The axisymmetric design before and after the optimization in FE software is presented in the first section. In this section, the effects on the field uniformity by different parametrizations are investigated. In the second section, the results from the three dimensional analysis are presented and a comparison is made between the magnetic fields before and after the optimization of the MRI device. In the third section, the mechanical analysis results are presented. The magnetic field of the MRI device is simulated in comsol multiphysics v5.3a using the magnetostatics module. The mechanical structure has been analyzed using the solid mechanics module of the same software.

4.1 2D axisymmetric model

In this section, a basic design in FEMM is introduced. The axisymmetric design is built using the FE software. The face of the pole piece is parametrized by using different control points which can vary along the axial direction. These control points are forced to keep the same position in the radial direction. The NURBs curve passes through these control points providing a smoother control to alter the shape of the pole piece. Before optimization, the pole piece face is produced using random parameters, and the corresponding axisymmetric field solution of the magnet assembly is shown in Fig. 17.

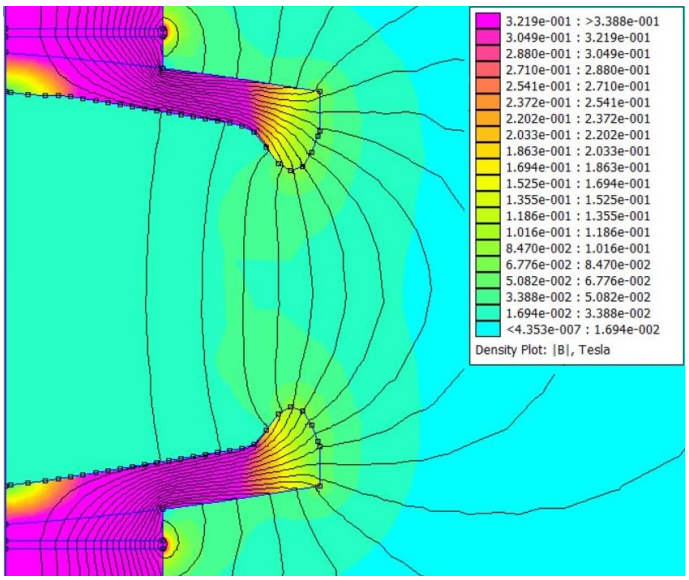

Fig. 17. Axisymmetric field solution in FEMM

The homogeneity value of the magnetic field is 2.5×10^5 PPM. The mass of the magnet and pole piece are 7kg and 310kg respectively. As this design lacks the magnetic field uniformity, the MRI device requires optimization through which this homogeneity value can be improved. The optimization results of the MRI device are presented in next section.

4.1.1 Optimized design in 2D

In this section, the results generated by the optimization algorithm are presented. Various designs for different parametrization of pole surface are evaluated and compared. The field intensity, uniformity, dimensions and weight of the magnet assembly are calculated for each parametrization. The dimensions of the magnet, yoke and the control points defining the pole surface are parametrized in the optimization algorithm. Initially, the pole surface is optimized by parametrizing eleven control points. Then the effect of reduced number of control points to optimize the design is also investigated. Five different cases with different parametrizations are investigated. The optimized design of those five cases showed that the pole faces generated by the reduced parametrization are smooth. The smooth pole faces are easy to manufacture for practical applications. Moreover, if the parameters are increased, the face generated by the optimization algorithm becomes increasingly uneven. As a result, with too many parameters it is difficult to manufacture due to the mechanical constraints. Furthermore, too many parameters increase the computation time significantly, however, it provides greater flexibility of exploring the unknown parts of the search space to get an optimal design. In case of few parameters, the search space is too constrained that it is difficult to seek an optimal shape that can produce a uniform field in the imaging region. The shape with an optimal number of parameters which is easy to manufacture and can generate uniform field can be chosen to build a real magnet assembly. The result generated by different parametrizations are presented in the following section.

4.1.2 3 points parametrization

In this method, the faces of the pole pieces are defined by three control points which are allowed to vary along the axial coordinate. The parameters of the optimized assembly and the corresponding flux density plot is presented in Table. 6 and Fig. 18. It can be observed that the face of the poles is smooth which is easy to manufacture. However, the homogeneity value is higher than the acceptable limits. As shown in Table. 6 the final design does not provide an optimized solution, as the solution region is constrained.

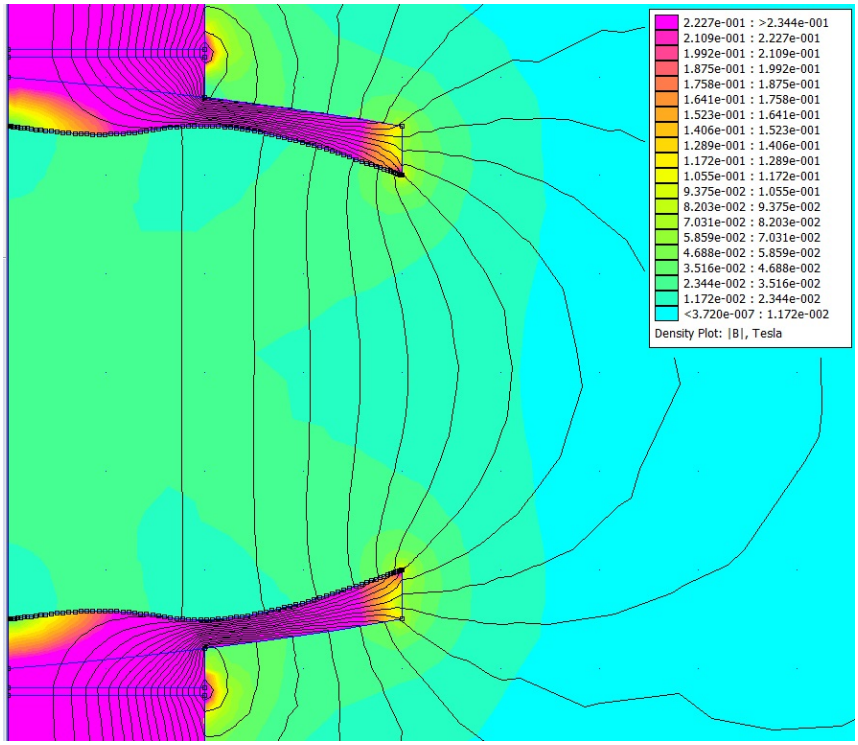

Fig. 18. Axisymmetric field solution for 3 points parametrization

Table 6: Parameters of 3 points parametrization

Parameters	**Values**
Field Strength(B)	19.9 mT
DSV	35cm
Homogeneity	7467 PPM
Diameter of magnet	30cm
Thickness of magnet	0.8cm
Weight of a magnet	4.4kg
Weight of pole piece	164kg
Weight of whole assembly	1730kg

4.1.3 5 Points parametrization

For five points parametrization, two different cases are studied. In the first case, the control points defining the pole surface are allowed to vary only along the axial coordinate, as for all the other cases. In the second case, we let the control points to vary along both coordinates (radial and axial) within the predefined search space. The results of both cases are given below.

4.1.3.1 Points fixed along the radial axis

The five points parametrization resulted in a smooth pole shape producing a uniform magnetic field with a minimum weight of the pole piece. The intensity of the magnetic field is 22mT in the measuring area. The parameters of the optimized assembly design and corresponding flux density plot are presented in Table. 7 and Fig. 19. The magnetic field uniformity is improved as compared to the three control points case. However, the algorithm is not able to achieve the high field uniformity with five points parametrization.

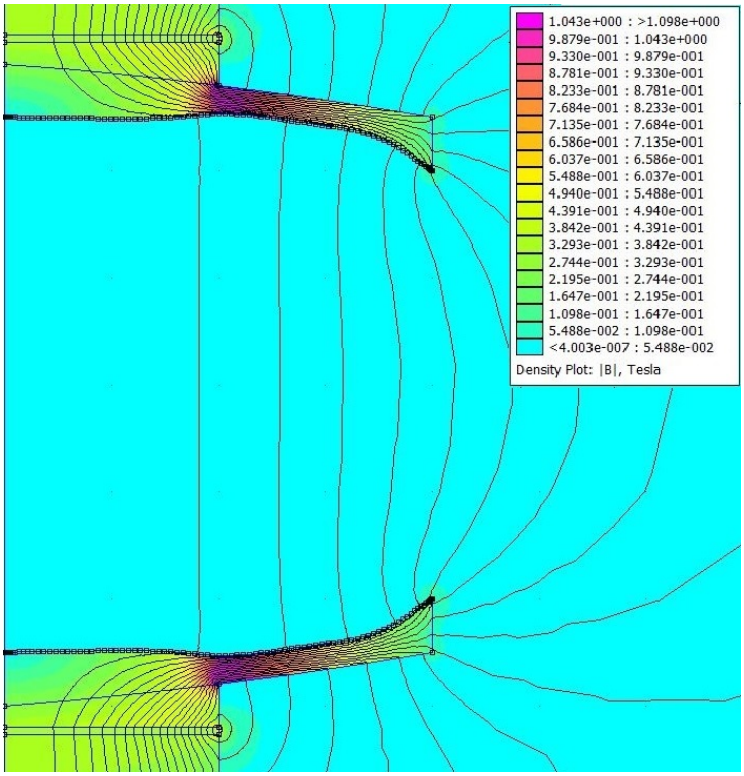

Fig. 19. Axisymmetric field solution for 5 points parametrization

Table 7: Parameters of 5 points parametrization

Parameters	**Values**
Field Strength(B)	22mT
DSV	35cm
Homogeneity	1148 PPM
Diameter of magnet	40cm
Thickness of magnet	0.75cm
Weight of a magnet	6.9kg
Weight of pole piece	152kg
Weight of whole assembly	2025kg

4.1.3.2 Points are allowed to vary along both coordinates

The pole surface is parametrized with five control points. The control points defining the pole surface are allowed to vary along both coordinates. The parameters of the optimized assembly design and the corresponding magnetic flux density plot is presented in Table. 8 and Fig. 20. The weight of the pole is increased while the uniformity of the field is decreased in comparison with the previous case. Thus, by allowing the control points to vary along both coordinates results in a wider solution region and the optimization algorithm stucks into a local optima. The accurate results are obtained by varying the control points in only one direction. Furthermore, the variation of the control points in both directions can degrade the results. Therefore, we will only consider the approach in which the control points are fixed along the radial axis.

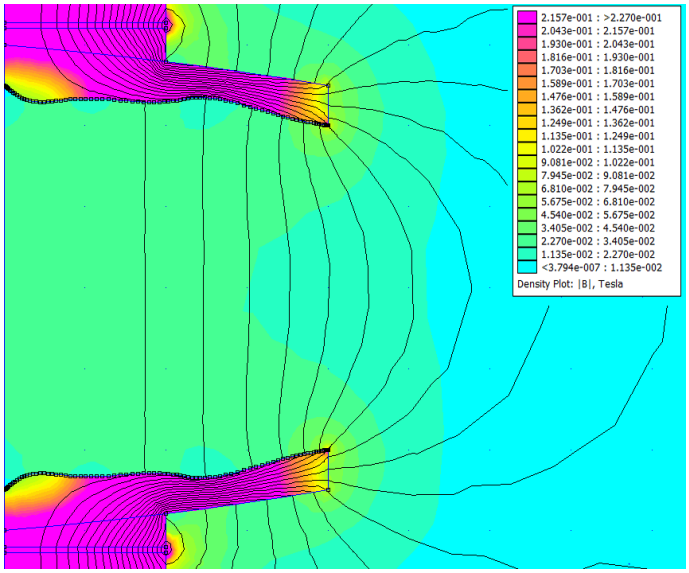

Fig. 20. Axisymmertic field solution of five points parametrization

Table 8: Parameters of 5 points parametrization

Parameters	**Values**
Field Strength(B)	23.5mT
DSV	35cm
Homogeneity	1681 PPM
Diameter of magnet	40cm
Thickness of magnet	0.70cm
Weight of a magnet	6.5kg
Weight of pole piece	219kg
Weight of whole assembly	2160kg

4.1.4 7 points parametrization

In this case, the pole faces are parametrized by seven control points. It can be observed that by increasing the number of parameters, the field uniformity is increased. However, this leads to the slightly uneven shape of the pole surface. In this case, the homogeneity of the magnetic field and the weight of the magnet assembly are within the acceptable limits. Furthermore, the optimized shape is feasible for the construction of an MRI device. Thus, this design can be employed for a real assembly design. The axisymmetric field solution is presented in Fig. 21 and optimized magnet assembly parameters are given in Table. 9.

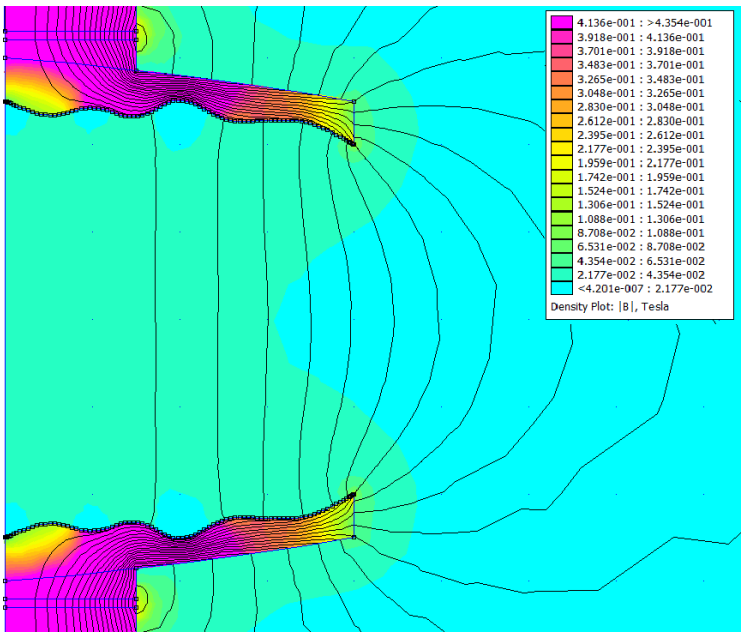

Fig. 21. Axisymmetric field solution for 7 points parametrization

Table 9: Parameters of 7 points parametrization

Parameters	**Values**
Field Strength(B)	23mT
DSV	35cm
Homogeneity	633 PPM
Diameter of magnet	30cm
Thickness of magnet	1cm
Weight of a magnet	5.23kg
Weight of pole piece	175kg
Weight of whole assembly	1754kg

4.1.5 9 Points parametrization

The pole face is optimized with nine control points. Optimizing the pole surface with nine parameters increases the computation time and results in an uneven surface of the pole. As already discussed, increasing the parameters increases the probability of finding a better design for the MRI device. In this case, the field uniformity and the intensity of the generated pole design is found easily in acceptable limits. The flux density plot and optimized design parameters are presented in Fig. 22 and Table. 10 respectively.

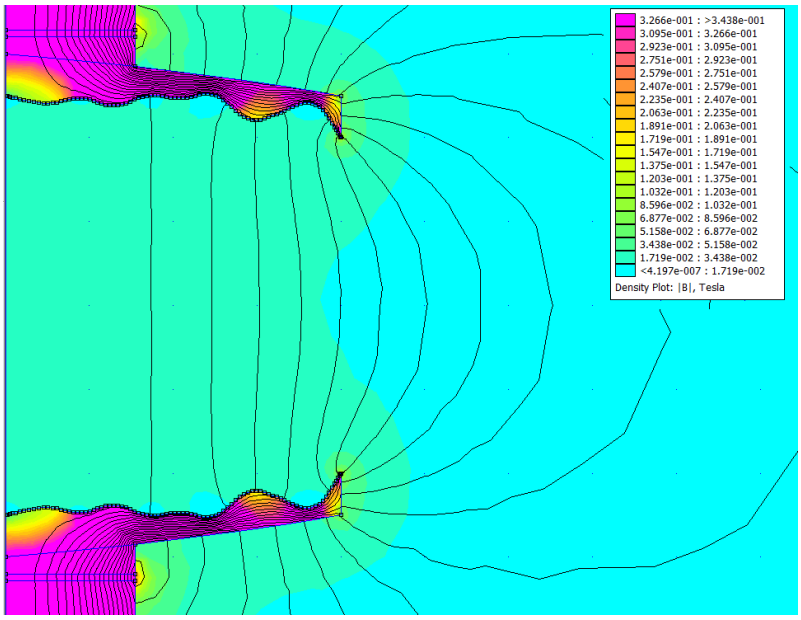

Fig. 22. Axisymmetric field solution for 9 points parametrization

Table 10: Parameters of 9 points parametrization

Parameters	**Values**
Field Strength(B)	20.1mT
DSV	35cm
Homogeneity	624 PPM
Diameter of magnet	31cm
Thickness of magnet	0.70cm
Weight of a magnet	4.3kg
Weight of pole piece	162kg
Weight of whole assembly	1723kg

4.1.6 11 Points parametrization

In this case, the pole surface is optimized with eleven control points. The results show that too many parameters not only increase the computational burden but can result in a haphazard bumpy surface of the pole which is impractical for a real assembly design. A much higher precision and accuracy is required to manufacture such shape for practical applications. In this case, the field uniformity is 557 PPM, however, the weight of the pole piece is increased. The magnetic flux density plot for 11 points parametrization is presented in Fig. 23. The parameters generated by the optimization algorithm are given in Table. 11.

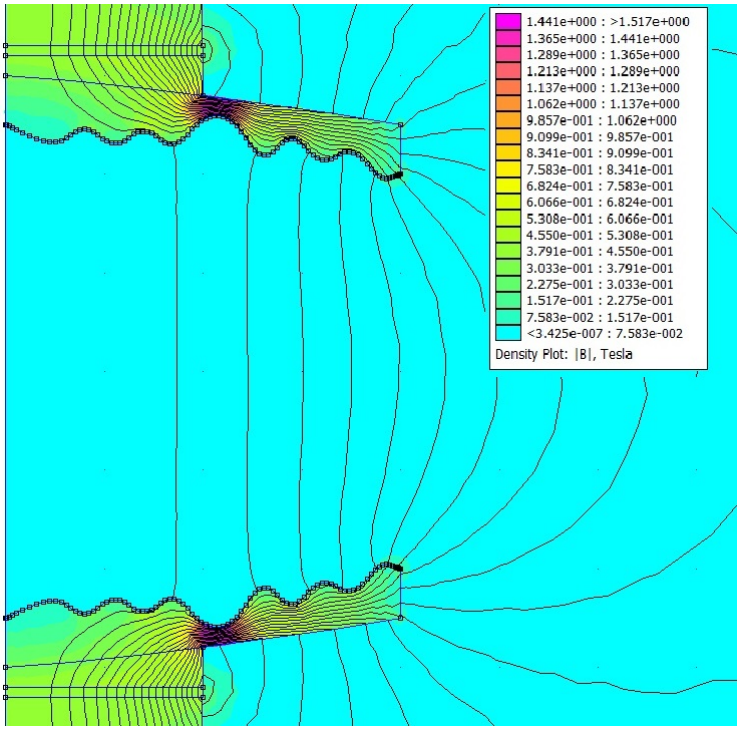

Fig. 23. Axisymmetric field solution for 11 points parametrization

Table 11: Parameters of 11 points parametrization

Parameters	**Values**
Field Strength(B)	21.9mT
DSV	35cm
Homogeneity	557 PPM
Diameter of magnet	40cm
Thickness of magnet	0.65cm
Weight of a magnet	6.2kg
Weight of pole piece	202.7kg
Weight of whole assembly	2130kg

4.1.7 Magnetic field computation

The magnetic field is computed at discrete points on a spherical volume. We defined eleven points equidistant from each other on a spherical volume to account for the homogeneity. The magnetic field uniformity is measured on various DSV's for all the parametrized shapes. The detailed results are provided in Table. 12.

Table 12: Homogeneity along various DSV's in PPM

Parameters	**35cm DSV**	**30cm DSV**	**25cm DSV**	**20cm DSV**	**15cm DSV**
3	7467	2144	1231	571	303
5	1148	619	162	53	28
7	633	576	157	63	37
9	624	360	162	84	60
11	556	410	206	45	11

The measured field is more uniform in the centre of the imaging area and as we move away from the centre, the uniformity of the magnetic field decreases. The initial design with some random parameters is not able to produce the uniform magnetic field. Thus, optimization is carried out to increase the field uniformity. The optimization algorithm increases the field uniformity by optimizing the pole surface, which further leads to the reduced weight of the poles and the magnets. However, the strength of the magnetic field is slightly decreased in comparison with the design before the optimization but it is still within the acceptable limits.

Apart from varying the number of parameters, the algorithm is tested by varying the search space. The wider solution region is achieved by increasing the boundary limits, which results in the increase of the computation time to achieve an optimal design. In this case, the wider solution region has direct effect on the thickness of the pole, which increases the weight of the pole. However, if the search space is made too constrained by decreasing the boundary limits, there is a possibility that the optimal solution may exist out of the search space. Thus, it is difficult to seek an optimal design with the constrained solution region.

The device with its support is not axisymmetric and there will be uneven flux leakage from the pole faces to the support, which might result in degraded homogeneity and decreased field strength in the imaging region. For this purpose, a 3D model is built in commercially available FE software. Details are presented in section 4.2.

4.2 3D electromagnetic analysis

The finalized geometry design is subjected to three dimensional analysis to account for the effect of the yoke on the uniformity of the magnetic field. The optimized magnet poles generated by the various parametrizations are implemented in 3D and are presented in Fig. 24. The 3D analysis results are in good agreement with the 2D analysis results on the nature of the magnetic field uniformity with respect to the number of control points.

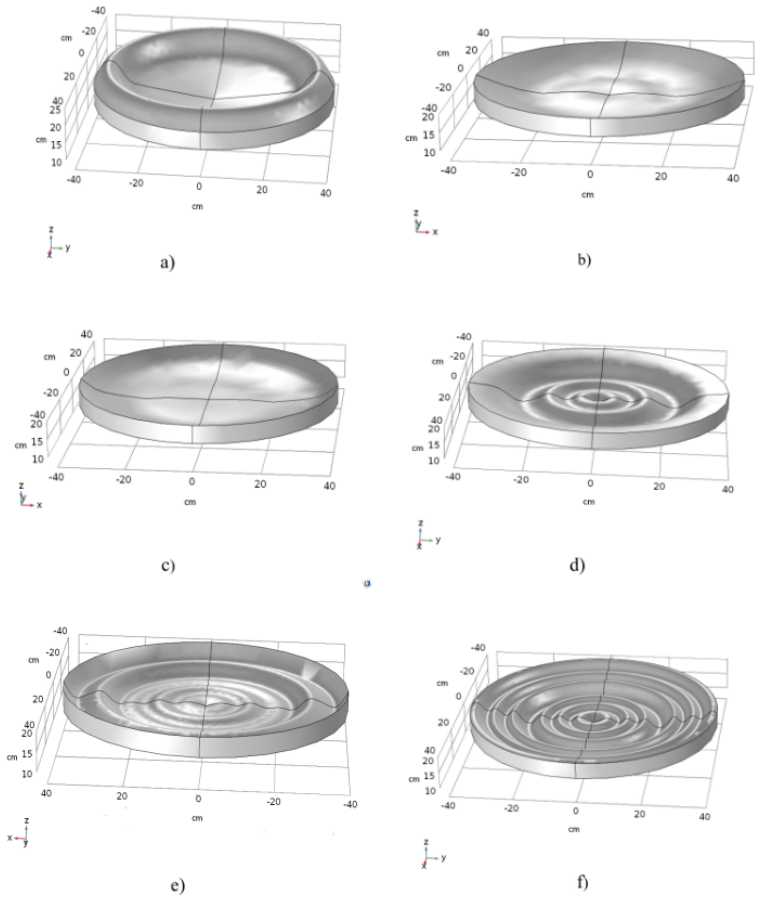

Fig. 24. Shapes of pole generated a) before optimization. b) optimized with 3 control points. c) optimized with 5 control points. d). optimized with 7 control points e). optimized with 9 control points f). optimized with 11 control points.

The yoke has a direct effect on the intensity of the magnetic field in the measuring area. It reduces the flux leakage by limiting it within a yoke (Bushong & Clarke 2014). To visualize the magnet flux distribution in a designed magnet assembly, the streamline plot of flux density is generated by using post processing toolbox of Comsol. The streamline plot is shown in Fig. 25, we can see from the streamlined plot that magnetic field lines are uniformly crossing the air gap while they vary abruptly if we move away from the centre.

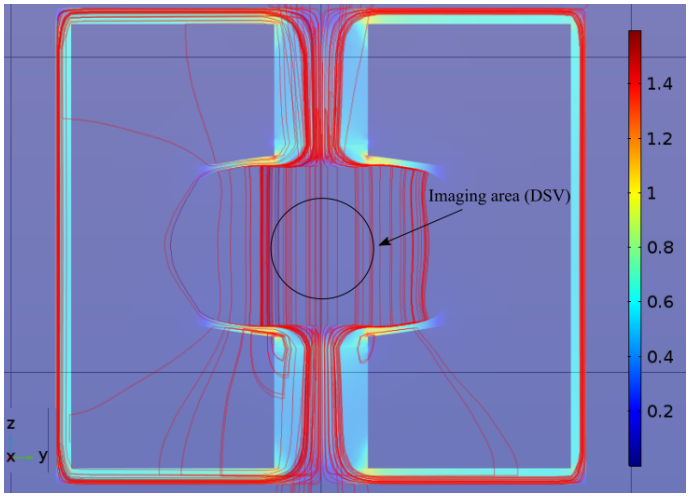

Fig. 25. Streamline plot of designed magnet assembly

To get a better understanding of the field behaviour in the imaging region, the magnetic flux density is measured in the imaging area. The flux density stays almost the same as that of 2D computation, which justifies our optimization approach. The comparison of the magnetic field before and after optimization for different parametrization is performed as shown in Fig. 26. The magnetic field in the imaging region is measured in xy plane (horizontal plane) for different positions along z-axis (vertical axis). The origin is assumed at the centre of the imaging area and is used as a reference for other measurements. Different measurement positions are presented in Table 13. It is clear from the results that shaping the pole surface significantly increases the magnetic field uniformity. Thus, based on the results the design optimized with seven control points is selected as an optimal design, which can produce the uniform magnetic field in the imaging region with the minimum weight of the assembly. Moreover, the pole face of the selected design can be easily manufactured.

Table 13: Different positions (Pos) of measurement in Imaging area.

Coordinates	**Pos. 1**	**Pos. 2**	**Pos. 3**	**Pos. 4**	**Pos. 5**	**Pos. 6**
x_1, x_2	-50, 50	-50, 50	-50, 50	-50, 50	-50, 50	-50, 50
y_1, y_2	0, 0	10, 10	0, 0	10, 10	0, 0	5, 5
z_1, z_2	10, 10	0, 0	0, 0	10, 10	5, 5	0, 0

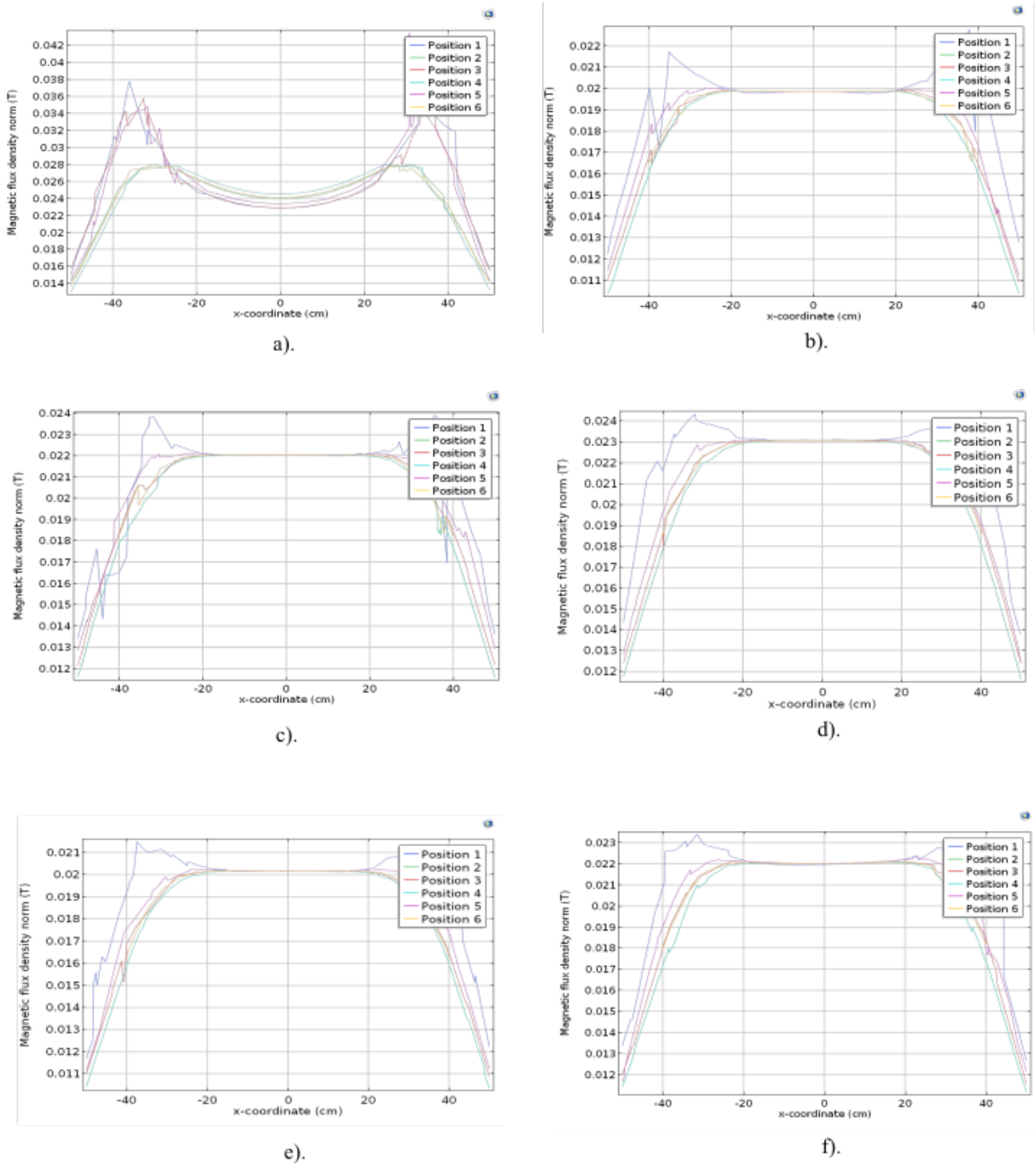

Fig. 26. Comparison of magnetic flux densities. a) Before optimization. b). Optimized with 3 parameters. c). Optimized with 5 parameters. d). Optimized with 7 parameters. e). Optimized with 9 parameters. f). Optimized with 11 parameters.

4.2.1 Sensitivity analysis

The impact of the control points on the field uniformity is tested for different parametrizations. Now to take into account the effect of magnetic field tolerances, the remanent flux density ($\boldsymbol{B}_r$) and the coercivity ($\boldsymbol{H}_c$) of the magnet is varied within a range of ±5% of the actual value. The magnetic field intensity and uniformity are measured in the imaging area and results are presented in Fig. 27-28, and Table. 14-15. The homogeneity of the magnetic field in the imaging area for different values of $\boldsymbol{B}_r$ and $\boldsymbol{H}_c$ remains the same, while the intensity of the magnetic field changes significantly.

Table 14: Effect of $\boldsymbol{B}_r$ on field strength

Remanent flux Density ($\boldsymbol{B}_r$)	Magnetic flux density ($\|\boldsymbol{B}\|$)
1.19 T	21.90 mT
1.26 T	23.08 mT
1.32 T	24.26 mT

Table 15: Effect of $\boldsymbol{H}_c$ on field strength

Coercivity ($\boldsymbol{H}_c$)	Magnetic flux density($\|\boldsymbol{B}\|$)
907 kA/m	21.33 mT
955 kA/m	22.40 mT
1000.27 kA/m	23.78 mT

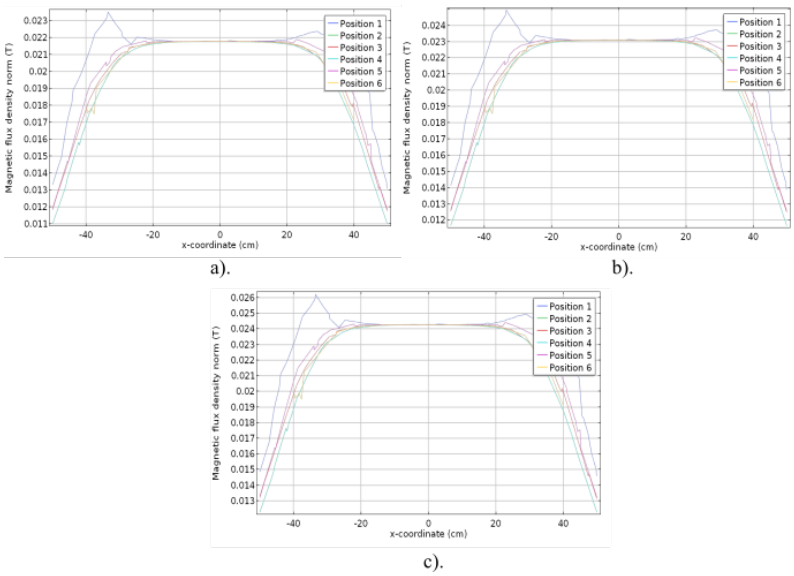

Fig. 27. Magnetic field in the imaging area. a) $\boldsymbol{B}_r$ =1.19T b) $\boldsymbol{B}_r$ =1.26T c) $\boldsymbol{B}_r$ =1.323T

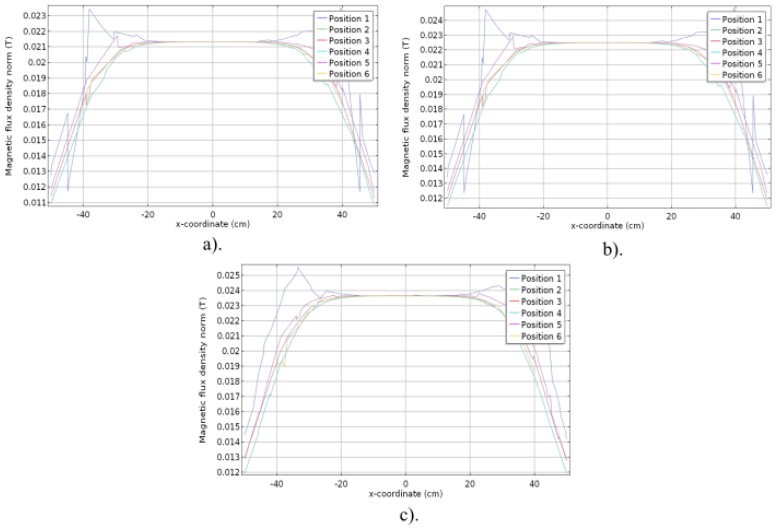

Fig. 28. Magnetic field in the imaging area. a) $\boldsymbol{H}_c$=907 kA/m b) $\boldsymbol{H}_c$=955 kA/m c) $\boldsymbol{H}_c$=1000.27 kA/m

4.3 3D mechanical analysis

To verify the stiffness of the designed mechanical structure, the model is analyzed using solid mechanics module of Comsol multiphysics. The weight of the beam, yoke and pole is taken into account to compute the total force acting on the model. Von Mises stress analysis is usually employed to check for the stability of a designed structure. For a given structure if the maximum loading causes a stress less then the yield stress value of that material, then it is considered as stable. The von Mises stress analysis is performed for our designed structure and it showed a maximum value of 12Mpa, which is much less than the yield stress of iron. The von Mises stress analysis is presented in Fig. 29.

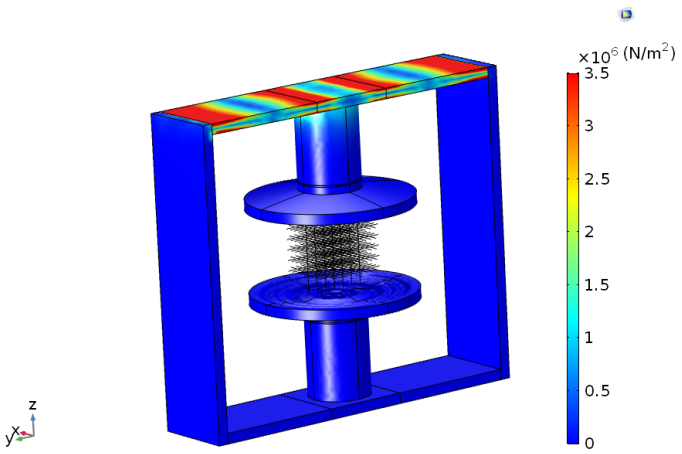

Fig. 29. von Mises Stress analysis

To further confirm the stability of a structure, the maximum displacement analysis is performed. The total displacement of 0.1mm in the upper pole is observed, which is shown in Fig. 30. The magnetic field in the imaging area is measured again by taking in to account the effect of displacement. The simulation results showed that the magnetic field intensity remains almost the same, but the field uniformity is disturbed by approximately 230 PPM. The field uniformity is disturbed due to the displacement of the pole. These magnetic field inhomogeneities can be corrected by implementing the other magnetic field correction methods (shimming) after the installation of the device. The magnetic flux density graph is shown in Fig. 31, which shows the behaviour of the magnetic field under the effect of displacement.

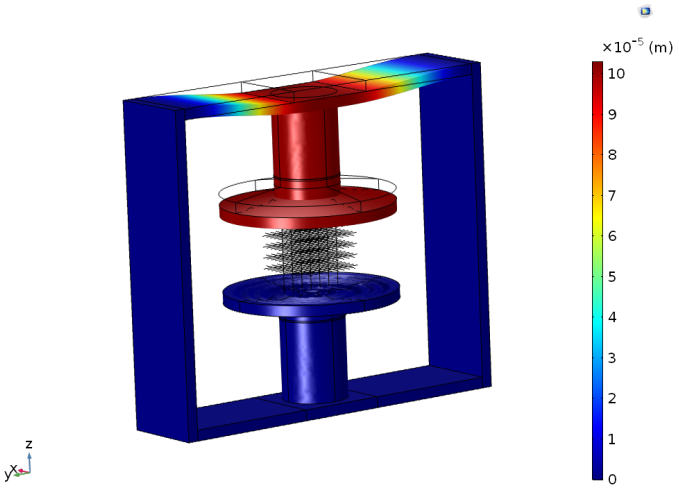

Fig. 30. Total displacement analysis (Scale factor: 500)

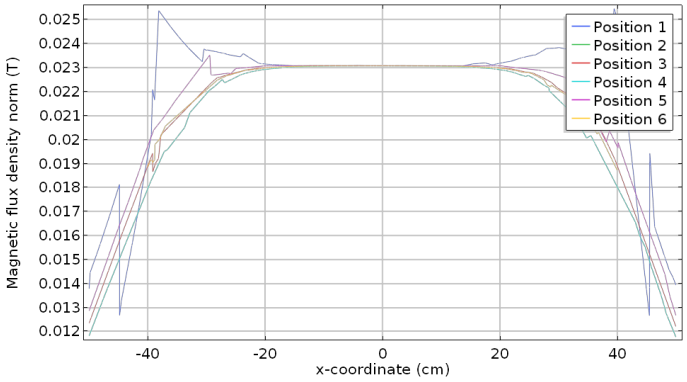

Fig. 31. Magnetic flux density of the imaging region

Chapter 5

5 Conclusion

In this thesis, a method for the design and optimization of the permanent magnet poles of an MRI device is studied. Initially, a design is developed in FEMM using Matlab's toolbox. Matlab's implemented design is linked to the optimization algorithm and a pole face is generated after several iterations producing the uniform magnetic field in the imaging region. Due to the optimization, the field uniformity increases significantly. The optimized design is not only capable of generating uniform field but also a significant reduction in the weight of the magnet assembly is observed.

The PSO algorithm is used to carry out the optimization of the designed magnet assembly. The optimization is performed for different parametrization of pole faces. It has been found that increasing or decreasing the number of control points defining the pole surface have a significant effect on the field uniformity, weight and smoothness of the pole. The reduced parameter optimization results in designing a pole surface that is easy to manufacture for real assembly design with a reduced weight. Increasing the number of design variables to parametrize the pole shape result in a more uniform field with a drawback of more complex shape and increased weight. Five different parametrizations are studied and the optimization with seven control points is concluded to be the best optimal one. The optimal design generated by such parametrization results in a uniform field with a minimum weight of the magnet, pole and assembly. The optimized design is analysed in 3D to account for the effect of the yoke on the field and the stiffness of the designed structure. The designed structure is further analyzed for displacement and von Mises stress analysis. The following analysis revealed that the designed structure is strong enough to sustain the weight of the magnet assembly. Hence, the simulation results show that the designed assembly can be used to build a real low field MRI device.

To conclude, overall objectives of the thesis are achieved. Based on the results, the pole faces produced by the optimization algorithm can be used to increase the uniformity of the magnetic field in the imaging area. On the other hand, optimization alone cannot bring the uniformity to the workable limits of MRI device. Thus, different magnetic field correction methods have to be implemented to get the desired uniformity of the magnetic field. In future, this work can be extended with the implementation of different shimming techniques, to get a higher field uniformity.

References

Anderson, W. A. (1961), 'Electrical current shims for correcting magnetic fields', *Review of Scientific Instruments* **32**(3), 241–250.

Blondin, J. (2009), 'Particle swarm optimization: A tutorial', *from site: http://cs. armstrong. edu/saad/csci8100/pso tutorial.pdf* . [Accessed 25 Feb 2018].

Bushong, S. C. & Clarke, G. (2014), *Magnetic resonance imaging: physical and biological principles*, Elsevier Health Sciences.

Calin, M.-D. & Helerea, E. (2011), Temperature influence on magnetic characteristics of NdFeB permanent magnets, *in* 'Advanced Topics in Electrical Engineering (ATEE), 2011 7th International Symposium on', IEEE, pp. 1–6.

Cheng, Y., He, W., Xia, L. & Liu, F. (2015), 'Design of shimming rings for small permanent mri magnet using sensitivity-analysis-based particle swarm optimization algorithm', *Journal of Medical and Biological Engineering* **35**(4), 448–454.

Cheng, Y., Xia, L., He, W., Liu, F. & Crozier, S. (2012), Design and Optimization of a Permanent Magnet for Small-sized MRI Based on Particle Swarm Optimization Algorithm, *in* '20th Annual Meeting of the International Society for Magnetic Resonance in Medicine (ISMRM)'.

Cheng, Y. Y., Xia, L. & He, W. (2013), Simulation and optimization of a permanent magnet for small-sized MRI by genetic algorithm, *in* 'Applied Mechanics and Materials', Vol. 341, Trans Tech Publ, pp. 577–580.

Fazanaro, D., Amorim, P., Moraes, T., Silva, J. & Pedrini, H. (2016), 'NURBS Parameterization for Medical Surface Reconstruction', (February), 137–144.

Frollo, I. & Strolka, P. (2001), 'Measuring method and magnetic field homogeneity optimisation for magnets used in nmr-imaging', *Measurement science review* **1**(1), 9–12.

Glover, F. (1986), 'Future paths for integer programming and links to artificial intelligence', *Computers & operations research* **13**(5), 533–549.

Haris Perlman, H. (1993), 'United States Patent, US6842002', **2**(12), 3–5.

Holland, J. (1975), 'Adaptation in artificial and natural systems', *Ann Arbor: The University of Michigan Press* .

Jiang, X., Shen, G., Lai, Y. & Tian, J. (2004), 'Development of an open 0.3 T NdFeB MRI magnet', *IEEE Transactions on Applied Superconductivity* **14**(2), 1621–1623.

Jie, S., Qin, X., Ying, L. & Gengying, L. (2005), 'Home-built magnetic resonance imaging system (0.3 t) with a complete digital spectrometer', *Review of scientific instruments* **76**(10), 105101.

Kennedy, J. & Eberhart, R. (1995), Particle swarm optimization, *in* 'Neural Networks, 1995. Proceedings., IEEE International Conference on', Vol. 4, pp. 1942–1948 vol.4.

Leonard, P. J. & Connor, A. M. (2000), 'Pole shape optimization using a tabu search scheme', *IEEE Transactions on Magnetics* **36**(4), 1115–1118.

Liu, Y. (2003), 'Effect of Knot Vectors on B-Spline Curves and Surfaces', *MEC Term Pap. 572* **0**(572), 1–14.

Meeker, D. (2010), 'Finite element method magnetics', *FEMM User Man.* (4.2). [Accessed 10 Nov 2017].
URL: *http://www.femm.info/Archives/doc/manual42.pdf*

Miyamoto, T., Sakurai, H., Takabayashi, H. & Aoki, M. (1989), 'A development of a permanent magnet assembly for MRI devices using Nd-Fe-B material', *IEEE Transactions on Magnetics* **25**(5), 3907–3909.

Miyamoto, T., Sakurai, H., Takabayashi, H. & Aoki, M. (1990), 'Development of a Permanent Magnet Assembly for MRI', *IEEE Translation Journal on Magnetics in Japan* **5**(9), 803–809.

Molfino, P., Repetto, M., Bixio, A., Mut, G. D. & Marabotto, R. (1988), 'Design of an axisymmetric permanent magnet structure for magnetic resonance tomography', *IEEE Transactions on Magnetics* **24**(2), 994–997.

Onnes, H. (1911), 'The superconductivity of mercury', *Leiden Comm* **120b, 122b, 124c**.

Peterson, J. (1990), 'Albert Technical Memo', pp. 1–8.

Piegl, L. (1991), 'On nurbs: a survey', *IEEE Computer Graphics and Applications* **11**(1), 55–71.

Podol'Skii, A. (2000), 'Design procedure for permanent magnet assemblies with uniform magnetic fields for mri devices', *IEEE transactions on magnetics* **36**(2), 484–490.

Ren, Z., Xie, D. & Li, H. (2009), 'Study on shimming method for open permanent magnet of mri', *Progress In Electromagnetics Research* **6**, 23–34.

Robinson, J. & Rahmat-Samii, Y. (2004), 'Particle swarm optimization in electromagnetics', *IEEE Transactions on Antennas and Propagation* **52**(2), 397–407.

Shi, Y. & Eberhart, R. C. (1999), Empirical study of particle swarm optimization, *in* 'Evolutionary computation, 1999. CEC 99. Proceedings of the 1999 congress on', Vol. 3, IEEE, pp. 1945–1950.

Tadic, T. & Fallone, B. G. (2010), 'Design and optimization of a novel bored biplanar permanent-magnet assembly for hybrid magnetic resonance imaging systems', *IEEE transactions on magnetics* **46**(12), 4052–4058.

Tadic, T. & Fallone, B. G. (2011), 'Three-dimensional nonaxisymmetric pole piece shape optimization for biplanar permanent-magnet mri systems', *IEEE Transactions on Magnetics* **47**(1), 231–238.

Trequattrini, A., Coscia, G. & Pittaluga, S. (2000), 'Double-cavity open permanent magnet for dedicated mri', *IEEE Transactions on Applied Superconductivity* **10**(1), 756–758.

Xin, T., Li-Ming, H. & Dong-Lin, Z. (2010), 'Active ferromagnetic shimming of the permanent magnet for magnetic resonance imaging scanner', *Chinese Physics B* **19**(7), 078702.

Yamamoto, S., Konii, K., Tanabe, H., Yokoyama, S., Matsuda, T. & Yamada, T. (2014), 'Super-stable superconducting mri magnet operating for 25 years', *IEEE Transactions on Applied Superconductivity* **24**(3), 1–4.

Yanli, Z., Dexin, X. & Pingchou, X. (2003), Passive shimming and shape optimization of an unconventional permanent magnet for MRI, *in* 'Electrical Machines and Systems, 2003. ICEMS 2003. Sixth International Conference on', Vol. 2, IEEE, pp. 899–902.

Yuan, W., Liu, Y., Wang, H. & Cao, Y. (2017), 'A geometric structure-based particle swarm optimization algorithm for multiobjective problems', *IEEE Transactions on Systems, Man, and Cybernetics: Systems* **47**(9), 2516–2537.

Zitzler, E., Laumanns, M. & Bleuler, S. (2004), A tutorial on evolutionary multiobjective optimization, *in* 'Metaheuristics for multiobjective optimisation', Springer, pp. 3–37.